CHAPTER 3
Structure design

3.1 Introduction

In this chapter, the theory of semiconductor heterojunction which has been mentioned in the previous chapter will be re-discussed in term of bandgap engineering. According to this concept, two types of staircase bandgap photodiode will be designed with difference tailored staircase bandgap in active region. The generation rate and the spectral response are then calculated and discussed comparing to the one of constant bandgap to optimize the designed structure.

3.2 Bandgap engineering

Refer to the section 2.2, 2.4 and 2.5 in the previous chapter, we can clearly define the term "bandgap engineering" which is the method of tailoring semiconductor band structure in order for some desired properties unattainable in homostructures. [24] The graded bandgap is one example that can be done by engineering the bandgap with gradually adjusting the chemical composition of the material varies with depth into the structure during the growth. This technique can be applied to the $Ga_{1-x}Al_xAs/GaAs$ heterostructures as shown in Fig. 3.1. The gradient of the band edge can produce the so-called "quasi-electric field" in a non-uniform semiconductor, the gradient of the conduction band edge need not to be the same as that of the valence band edge. Therefore, the quasi-electric field which acts upon electrons can be different from the quasi-electric field that acts upon holes, leading to certain effects that would not possible in a strictly uniform semiconductor. [15]

The purpose of this research is to apply a staircase bandgap structure into the PIN photodiode to produce the quasi-electric field, especially in active region. For the sake of this: (1) electrons and holes are then separated without any external electromotive force → high-efficiency photovoltaic effect (2) the built-in quasi-electric field of conduction band edge and valence band edge can be separately adjusted → low noise avalanche photo diode (Avalanche Photo Diode: APD). To support this idea, therefore we design three groups of phototodiode: the constant bandgap structure (reference), the type A staircase bandgap structure and the type B staircase bandgap structure as shown in Fig. 3.2. By using the spectral response simulation, the optimal thickness of $Ga_{0.6}Al_{0.4}As$ (P^+) and GaAs (n^-) layer in the reference structure will hereafter be determined. These thicknesses will also be applied to other groups. The discussion of each group together with its properties: (1) spectral response simulation (2) generation rate calculations and (3) band diagram, will report in the next sections.

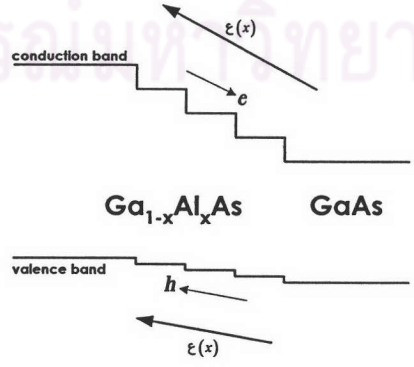

Fig. 3.1 Band diagram of the $Ga_{1-x}Al_xAs/GaAs$ heterostructure according to the bandgap engineering concept

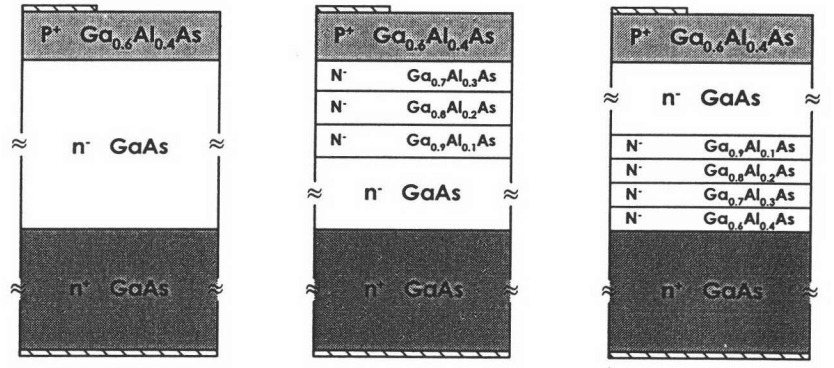

Constant bandgap (Reference) **Staircase bandgap (Type A)** **Staircase bandgap (Type B)**

Fig. 3.2 Conceptual structures

3.3 Spectral response simulation

The spectral response simulation is based upon the operation of PIN photodiode as mentioned in the previous chapter by using Matlab program. The incident light power is assumed to be constant at 3.5 x 10^{-5} Watt at all wavelengths. Moreover, the thermal generation within the depletion region is negligible and also the internal quantum efficiency is set to unity.

Firstly, we focus on finding the optimal thickness of GaAs (n^-) active layer by varying its thickness from 0.5 to 10 μm to obtain the suitable spectral response from the constant bandgap structure as shown in Fig. 3.3.

From the cutoff wavelength of $Ga_{0.6}Al_{0.4}As$ in Table 3.1, the theoretical spectral response of the constant bandgap window layer structure in Fig. 3.3, should actually rise up from the wavelength of nearly 644 nm, but it is not the case. For the reason that the $Ga_{0.6}Al_{0.4}As$ layer is not thick enough to absorb all of the optical power at this wavelength even though the absorption coefficient of this layer is high (see also in equation 2.53). Therefore, some photons can pass to the active region and contribute to the drift current. As for the spectral response between ~644 to ~870 nm, the thicker the GaAs (n^-) layer is, the better the optical power is absorbed. Anyway, the cutoff wavelengths of all different active layer thicknesses are approximately 870 nm, which is corresponding to the theoretical spectral response of GaAs. Up to this point, it is reasonable to say that the 6 μm GaAs active layer is suitable for our application.

Next, we pay attention to suppress the optical current originated from the photons with energy larger than that of window layer bandgap $\left(E > \frac{1240}{644nm}\ eV\right)$ and can penetrate to active layer, as mention in the previous paragraph. By varying the window layer thickness from 0.5 to 2.0 μm, the contribution of drift current in this range considerably decreases but become less and less when the window layer thickness is more than 2 μm. This layer thickness is therefore chosen for our application.

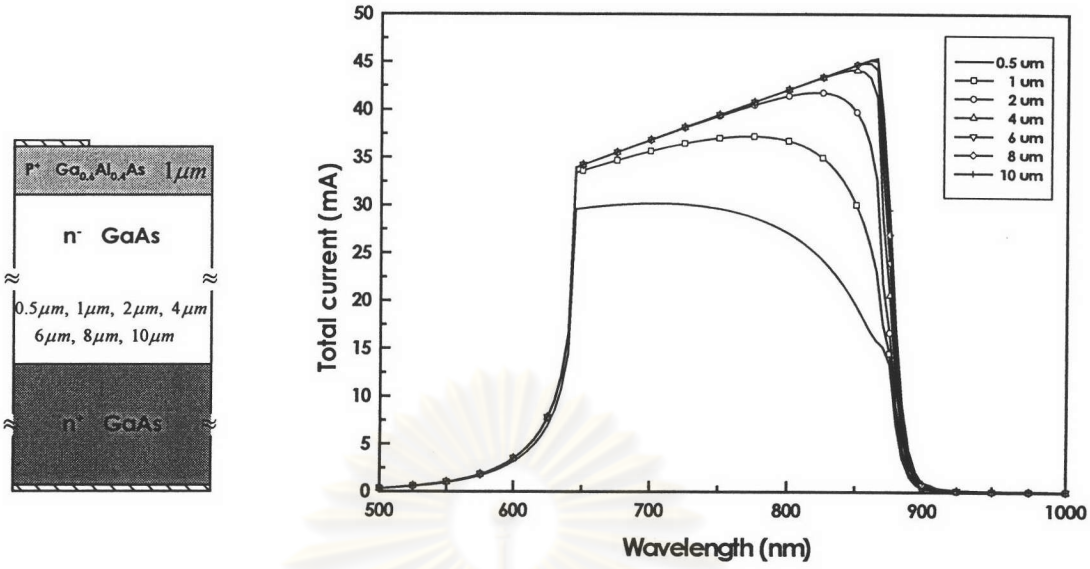

Fig. 3.3 Calculated spectral response of the 1 μm $Ga_{0.6}Al_{0.4}As$ (P^+) window layer photodiode with different GaAs (n^-) active layer thickness

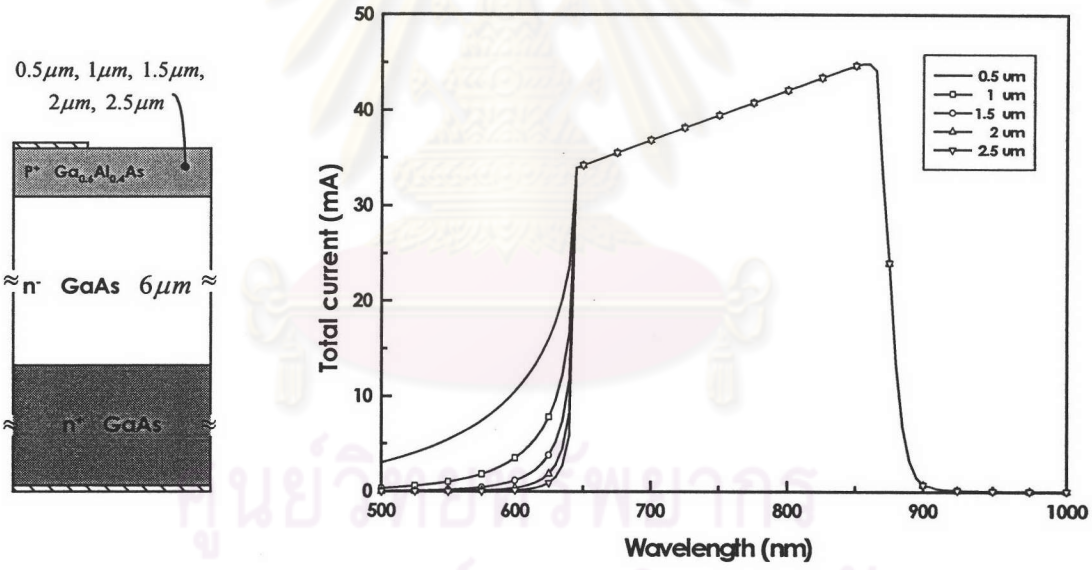

Fig. 3.4 Calculated spectral response of the 6 μm GaAs (n^-) active layer photodiode with different $Ga_{0.6}Al_{0.4}As$ (P^+) window layer thickness

Compounds	E_g(eV)	Wavelength(nm)
GaAs	1.425	870.175
$Ga_{0.9}Al_{0.1}As$	1.550	800.155
$Ga_{0.8}Al_{0.2}As$	1.674	740.564
$Ga_{0.7}Al_{0.3}As$	1.799	689.234
$Ga_{0.6}Al_{0.4}As$	1.924	644.558

Table 3.1 Bandgap energy and cutoff wavelength of GaAs and $Ga_{1-x}Al_xAs$

3.4 Structure Design

The parameters for constructing the band diagram according to Anderson's Model are shown in table 3.2. They are based upon the LPE's background carrier concentration N_D of 10^{15} cm^{-3} and the density of acceptor impurity atoms (N_A) is set at 10^{19} cm^{-3} for $Ga_{1-x}Al_xAs$ and 10^{18} cm^{-3} for GaAs. From these parameter values, three groups of structure have been designed: (1) constant bandgap structure (reference) (2) type A staircase bandgap structure and (3) type B staircase bandgap structure. Each structure will be discussed in the following sub-section.

Compounds \ Parameters			E_g(eV)	χ_e(eV)	n_i(cm^{-3})	N_A(cm^{-3})	N_D(cm^{-3})	E_F-E_i(eV)	E_F-E_V(eV)	ε_r	ϕ(ev)
p^+	GaAs		1.425	4.07	2.10E+06	1.00E+18	0	-0.696	0.016	13.180	5.479
n^+	GaAs		1.425	4.07	2.10E+06	0	1.00E+18	0.696	1.409	13.180	4.086
n^-	GaAs		1.425	4.07	2.10E+06	0	1.00E+15	0.518	1.230	13.180	4.265
p^+	$Ga_{1-x}Al_xAs$	0.1	1.550	3.96	2.24E+05	1.00E+18	0	-0.754	0.020	12.868	5.489
		0.2	1.674	3.85	2.26E+04	1.00E+18	0	-0.814	0.023	12.556	5.501
		0.3	1.799	3.74	2.27E+03	1.00E+18	0	-0.873	0.026	12.244	5.513
		0.4	1.924	3.63	2.26E+02	1.00E+18	0	-0.933	0.029	11.932	5.525
N^-	$Ga_{1-x}Al_xAs$	0.1	1.550	3.96	2.24E+05	0	1.00E+15	0.575	1.350	12.868	4.159
		0.2	1.674	3.85	2.26E+04	0	1.00E+15	0.635	1.472	12.556	4.052
		0.3	1.799	3.74	2.27E+03	0	1.00E+15	0.694	1.594	12.244	3.945
		0.4	1.924	3.63	2.26E+02	0	1.00E+15	0.754	1.716	11.932	3.838

Heterojunctions				ΔE_C(eV)	ΔE_V(eV)	qVb_1(eV)	qVb_2(eV)	qVb_2(eV)	x_1(cm)	x_2(cm)	W (cm)
p^+	p^+	$Ga_{0.6}Al_{0.4}As$	$Ga_{0.7}Al_{0.3}As$	0.110	0.015	0.012	0.006	0.006	2.844E-07	2.844E-07	5.688E-07
p^+	p^+	$Ga_{0.7}Al_{0.3}As$	$Ga_{0.8}Al_{0.2}As$	0.110	0.015	0.012	0.006	0.006	2.853E-07	2.853E-07	5.706E-07
p^+	p^+	$Ga_{0.8}Al_{0.2}As$	$Ga_{0.9}Al_{0.1}As$	0.110	0.015	0.012	0.006	0.006	2.875E-07	2.875E-07	5.750E-07
p^+	p^+	$Ga_{0.9}Al_{0.1}As$	GaAs	0.110	0.015	0.010	0.005	0.005	2.726E-07	2.726E-07	5.452E-07
p^+	n^-	$Ga_{0.6}Al_{0.4}As$	$Ga_{0.6}Al_{0.4}As$	0	0	1.687	1.686E-03	1.686	1.492E-07	4.717E-06	4.866E-06
p^+	n^-	$Ga_{0.6}Al_{0.4}As$	$Ga_{0.7}Al_{0.3}As$	0.110	0.015	1.580	1.619E-03	1.578	1.462E-07	4.624E-06	4.770E-06
p^+	n^-	$Ga_{0.7}Al_{0.3}As$	$Ga_{0.8}Al_{0.2}As$	0.110	0.015	1.461	1.496E-03	1.459	1.424E-07	1.424E-04	1.425E-04
p^+	n^-	$Ga_{0.8}Al_{0.2}As$	$Ga_{0.9}Al_{0.1}As$	0.110	0.015	1.342	1.374E-03	1.340	1.381E-07	1.381E-04	1.382E-04
p^+	n^-	$Ga_{0.9}Al_{0.1}As$	GaAs	0.110	0.015	1.224	1.253E-03	1.223	1.335E-07	1.335E-04	1.336E-04
p^+	n^-	$Ga_{0.8}Al_{0.2}As$	GaAs	0.220	0.029	1.236	1.296E-03	1.235	1.342E-07	1.342E-04	1.343E-04
p^+	n^-	$Ga_{0.7}Al_{0.3}As$	GaAs	0.330	0.044	1.248	1.342E-03	1.247	1.348E-07	1.348E-04	1.349E-04
p^+	n^-	$Ga_{0.6}Al_{0.4}As$	GaAs	0.440	0.059	1.260	1.390E-03	1.259	1.355E-07	1.355E-04	1.356E-04
p^+	n^-	GaAs	GaAs	0	0	1.214	0.001	1.213	1.330E-07	1.330E-04	1.331E-04
N^-	n^-	$Ga_{0.6}Al_{0.4}As$	$Ga_{0.7}Al_{0.3}As$	0.110	0.015	0.107	0.054	0.053	2.680E-05	2.680E-05	5.360E-05
N^-	n^-	$Ga_{0.7}Al_{0.3}As$	$Ga_{0.8}Al_{0.2}As$	0.110	0.015	0.107	0.054	0.053	2.711E-05	2.711E-05	5.422E-05
N^-	n^-	$Ga_{0.8}Al_{0.2}As$	$Ga_{0.9}Al_{0.1}As$	0.110	0.015	0.107	0.054	0.053	2.743E-05	2.743E-05	5.486E-05
N^-	n^-	$Ga_{0.9}Al_{0.1}As$	GaAs	0.110	0.015	0.106	0.053	0.052	2.758E-05	2.758E-05	5.516E-05
n^-	N^-	GaAs	$Ga_{0.9}Al_{0.1}As$	0.110	0.015	0.106	0.052	0.053	2.758E-05	2.758E-05	5.516E-05
n^-	N^-	$Ga_{0.9}Al_{0.1}As$	$Ga_{0.8}Al_{0.2}As$	0.110	0.015	0.107	0.053	0.054	2.743E-05	2.743E-05	5.486E-05
n^-	N^-	$Ga_{0.8}Al_{0.2}As$	$Ga_{0.7}Al_{0.3}As$	0.110	0.015	0.107	0.053	0.054	2.711E-05	2.711E-05	5.422E-05
n^-	N^-	$Ga_{0.7}Al_{0.3}As$	$Ga_{0.6}Al_{0.4}As$	0.110	0.015	0.107	0.053	0.054	2.680E-05	2.680E-05	5.360E-05
N^-	n^+	$Ga_{0.6}Al_{0.4}As$	GaAs	0.440	0.059	0.248	0.248	2.246E-04	5.723E-05	5.723E-08	5.729E-05
N^-	n^+	$Ga_{0.9}Al_{0.1}As$	GaAs	0.110	0.015	0.073	0.073	7.149E-05	3.229E-05	3.229E-08	3.232E-05
n^-	n^+	GaAs	GaAs	0	0	0.179	0.179	1.787E-04	5.105E-05	5.105E-08	5.110E-05

Table 3.2 The parameters for constructing the band diagram according to Anderson's Model

3.4.1 Constant bandgap structure (Reference)

The designed structure of constant bandgap is shown in Fig. 3.5. We illustrate the generation rate at the wavelengths of 635, 675, 725, 785 and 850 nm in Fig. 3.6 to have an understanding of the optical absorption mechanism. The optical power of 635 nm is very much absorbed inside the surface layer and decreases exponentially with depth until the interface of $Ga_{0.6}Al_{0.4}As$ and GaAs. Since the absorption coefficient of GaAs is higher, the generation rate therefore shifts up but not as high as the beginning before exponentially decreasing again. Such generation occurring inside the active region produces the drift current as seen in the spectral response of wavelength below 644 nm (see Fig. 3.7). As for the case of 675, 725,785 and 850 nm, there are little bits of absorptions in the $Ga_{0.6}Al_{0.4}As$ window layer with the generation rate around 10^{17} photons/sec/cm. Therefore, the optical power can penetrate to the active layer and are then completely absorbed. Furthermore, the generation rate is higher for the case of shorter wavelength owing to its higher absorption coefficient but it decreases exponentially with depth more rapidly. Hence, under the assumption that $\eta_i = 1$ and reverse bias voltage drops almost entirely across the n^- region, the total current as depicted in Fig. 3.7 can then be calculated by integrating G(x) generating inside the shaded area, as expressed in Fig. 3.6.

The band diagram of the constant bandgap structure is shown in Fig. 3.8. The conduction band gradient at the interface of GaAs (n^-) and GaAs (n^+) helps the electrons from the active region drift toward the n-side. Similarly, the valence band gradient at the interface of GaAs (n^-) and $Ga_{0.6}Al_{0.4}As$ (p^+) helps the holes flow easily to the p-side. However, the active region itself does not have any bandedge variation, which can produced the quasi-electric field to enhance the drift velocity.

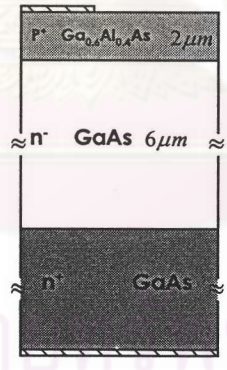

Fig. 3.5 The designed structure of constant bandgap

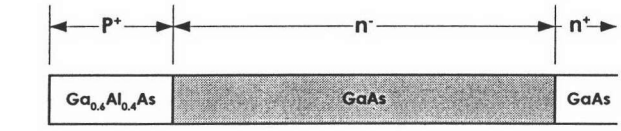

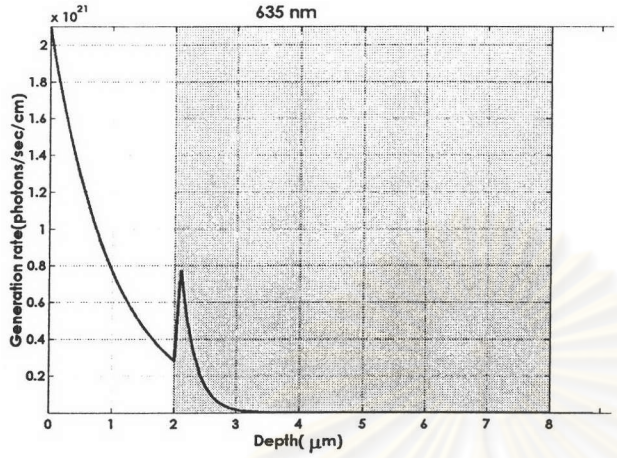

$$J_{dr}(635nm) = -q\int_{2\mu m}^{8\mu m} G(x)dx$$

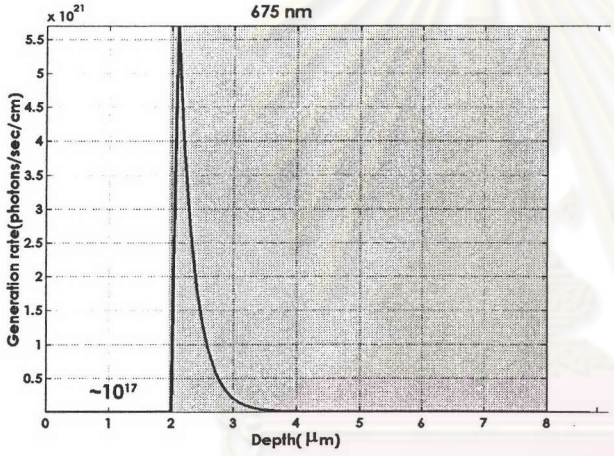

$$J_{dr}(675nm) = -q\int_{2\mu m}^{8\mu m} G(x)dx$$

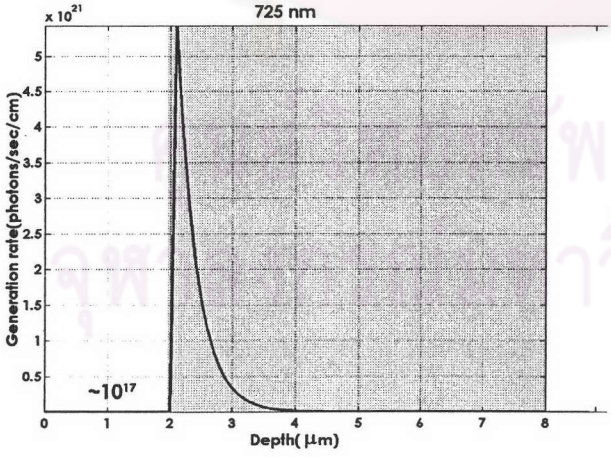

$$J_{dr}(725nm) = -q\int_{2\mu m}^{8\mu m} G(x)dx$$

Fig. 3.6 The EHPs generation rate at 635, 675, 725, 785 and 850 nm of constant bandgap structure

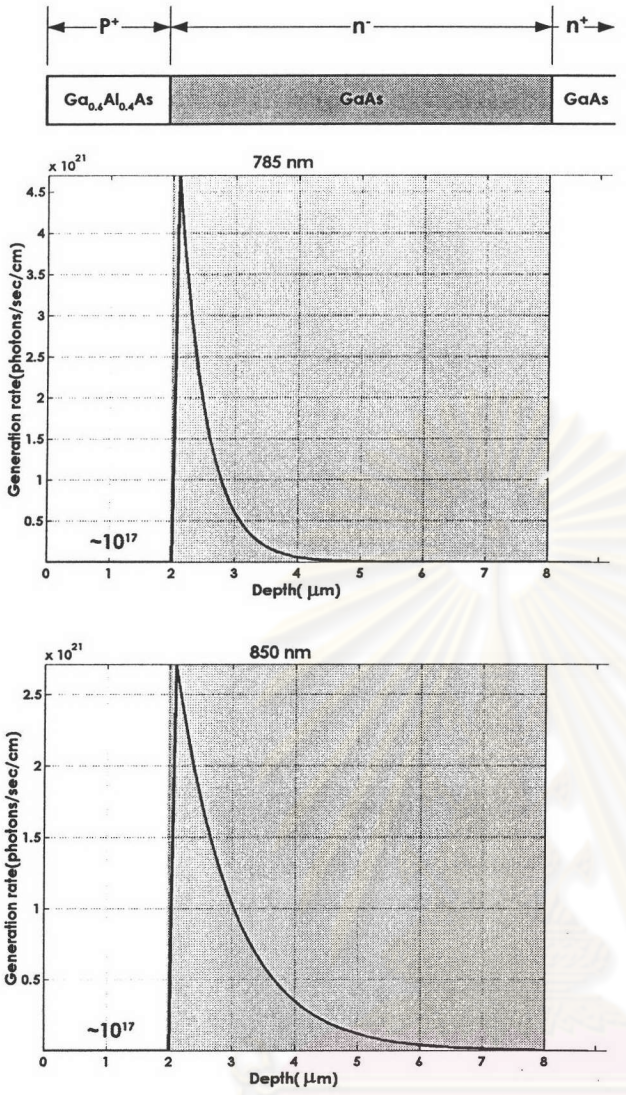

$$J_{dr}(785nm) = -q\int_{2\mu m}^{8\mu m} G(x)dx$$

$$J_{dr}(850nm) = -q\int_{2\mu m}^{8\mu m} G(x)dx$$

Fig. 3.6 (Continued)

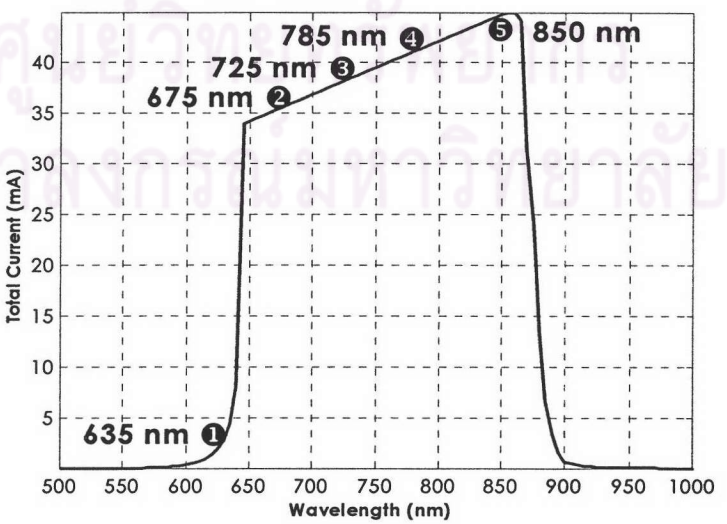

Fig. 3.7 The calculated spectral response of constant bandgap structure

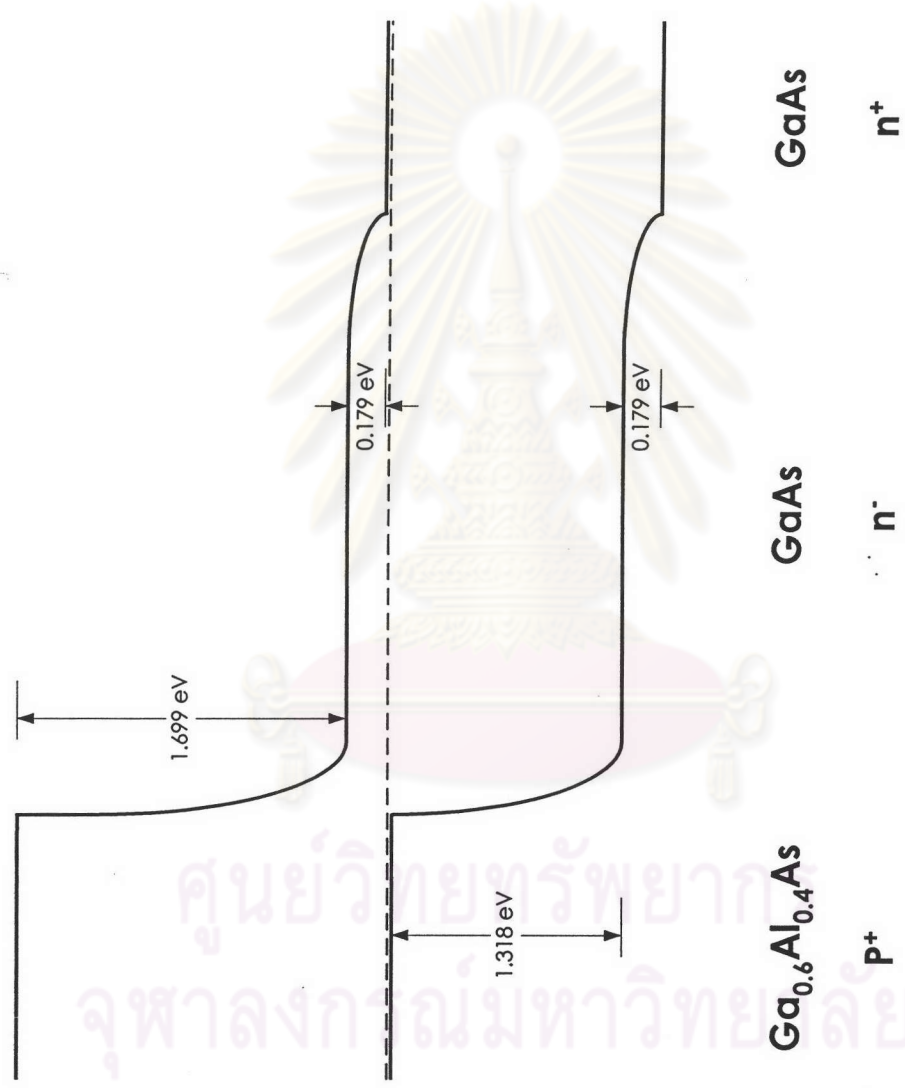

Fig. 3.8 The band diagram of constant bandgap structure

3.4.2 Type A staircase bandgap structure

The type A staircase bandgap structure is classified into four namely: Structure A1, Structure A2, Structure A3 and Structure A4 as shown in Fig. 3.9. The objective of these structures is to converge the bandgap energy of active layer from that of window layer to that of GaAs (n^+) substrate. The active layer of each structure is composed of $Ga_{0.7}Al_{0.3}As$, $Ga_{0.8}Al_{0.2}As$, $Ga_{0.9}Al_{0.1}As$ and GaAs in sequence from the top and with different thickness but all are doped at 10^{15} cm^{-3}. According to structure A1 to A4 in order, the thickness of GaAs (n^-) layer is adjusted to be 1.5 μm thicker for a time from 0 to 4.5 μm while the thickness of $Ga_{1-x}Al_xAs$ is adjusted to be 0.5 μm thinner for a time from 2 to 0.5 μm. However, the thickness of the window layer and the total active layer are respectively remained at 2 and 6 μm.

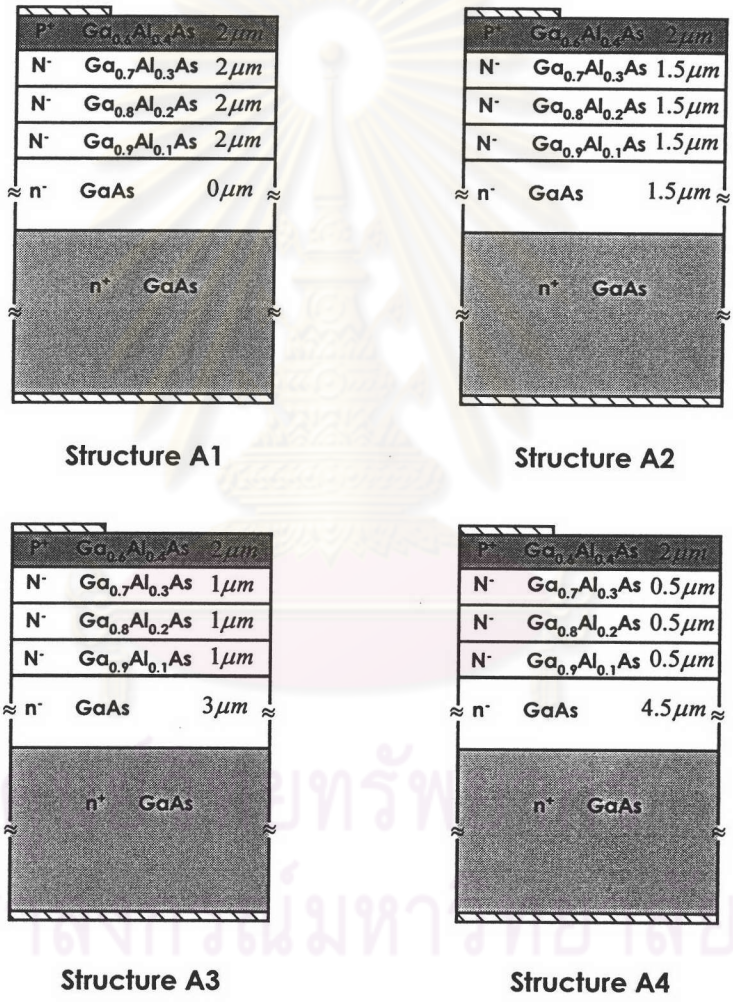

Fig. 3.9 Type A staircase bandgap structure

3.4.2.1 The calculated EHPs generation rate

To have an understanding of the optical absorption mechanism, the generation rates are again calculated at 635, 675, 725, 785 and 850 nm for every structure to compare to the one of constant bandgap. The calculated results are depicted in Fig. 3.10 to 3.13 for structure A1 to A4 respectively. The distribution of these generation rates will be discussed and compared to each other as follows:

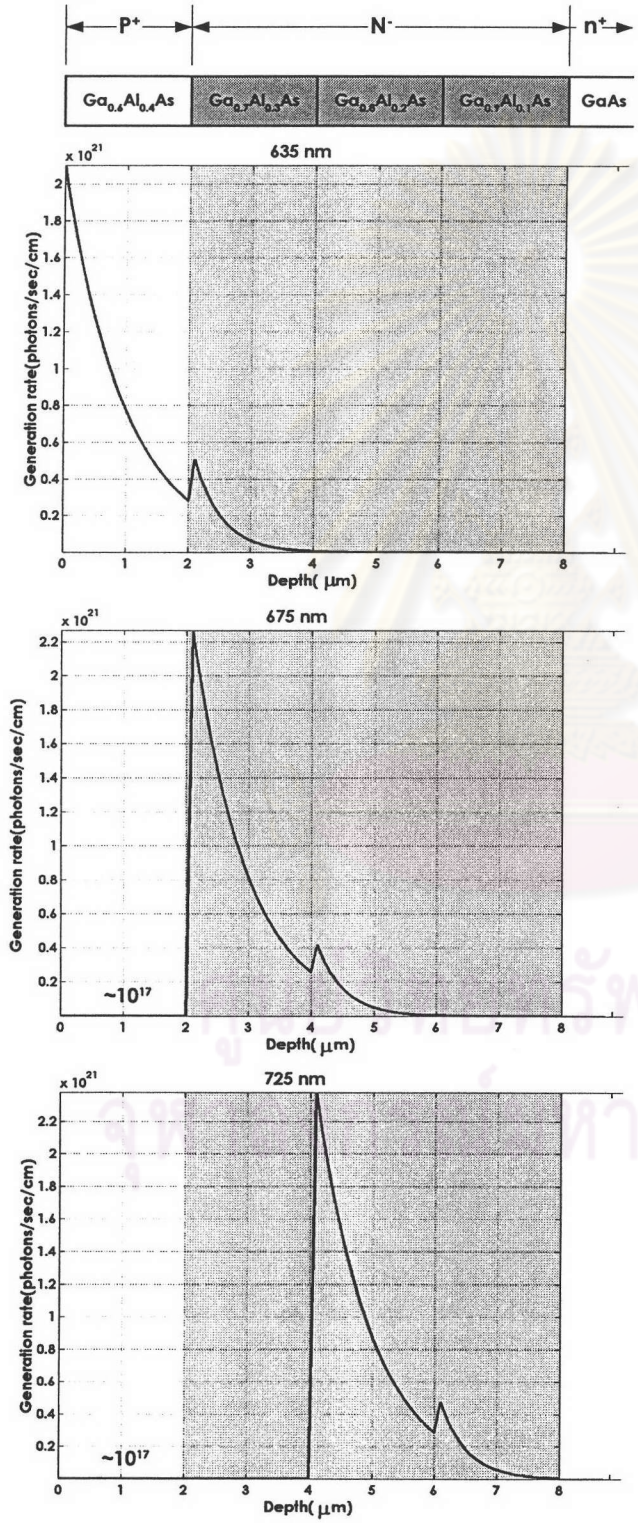

$$J_{dr}(635nm) = -q\int_{2\,\mu m}^{8\,\mu m} G(x)dx$$

$$J_{dr}(675nm) = -q\int_{2\,\mu m}^{8\,\mu m} G(x)dx$$

$$J_{dr}(725nm) = -q\int_{2\,\mu m}^{8\,\mu m} G(x)dx$$

Fig. 3.10 The EHPs generation rate at 635, 675, 725, 785 and 850 nm of structure A1

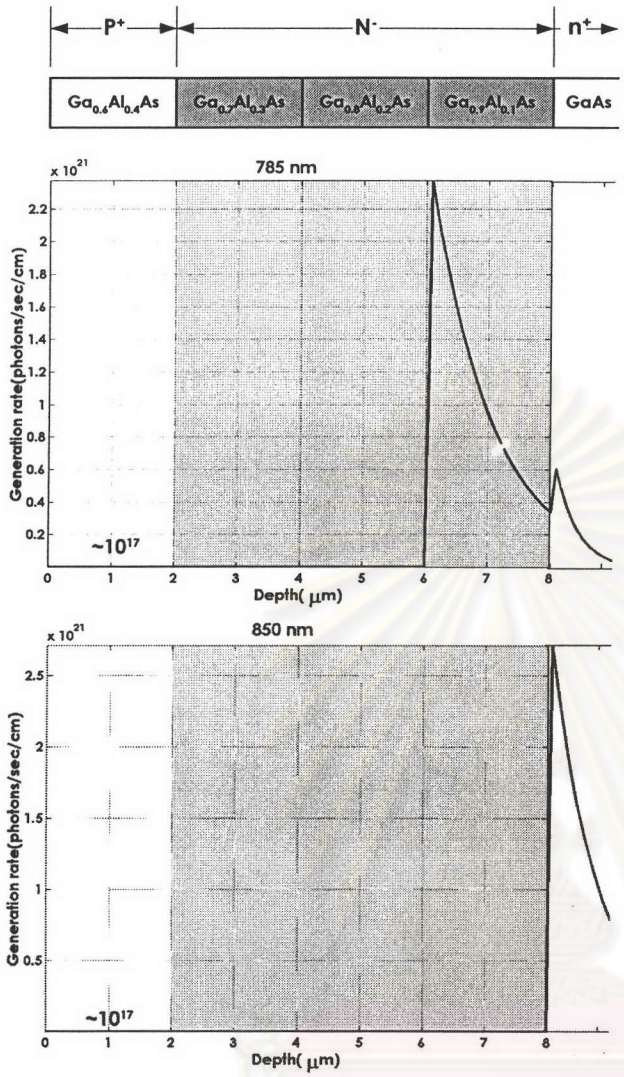

$$J_{dr}(785nm) = -q\int_{2\mu m}^{8\mu m} G(x)dx$$

$$J_{dr}(850nm) = -q\int_{2\mu m}^{8\mu m} G(x)dx$$

Fig. 3.10 (Continued)

Structure A1

In this structure, the 635 nm optical power of is very much absorbed inside the surface layer and decreases exponentially with depth as the one of the constant bandgap structure (reference structure) until the interface of $Ga_{0.6}Al_{0.4}As$ and $Ga_{0.7}Al_{0.3}As$. Since the absorption coefficient of $Ga_{0.7}Al_{0.3}As$ is lower than that of the GaAs, therefore the generation rate in the first 2 μm of active layer is therefore shifted up less than that of the reference structure and then decreased exponentially again but more slowly. For the reason that the absorption coefficient of staircase bandgap active layer increases step by step from that of $Ga_{0.6}Al_{0.4}As$ to that of $Ga_{0.9}Al_{0.1}As$, the generation rates of 675, 725 and 785 nm are again similar to the one of 635 nm. It is clear that the longer the wavelength is, the deeper the EHPs generate. Therefore, some photons of 785 nm are not absorbed in active region but penetrated into the substrate. Whereas the 850 nm photons would prefer to pass into the substrate more than to be absorbed in the active region because the structure A1 does not have the GaAs (n^-) active layer.

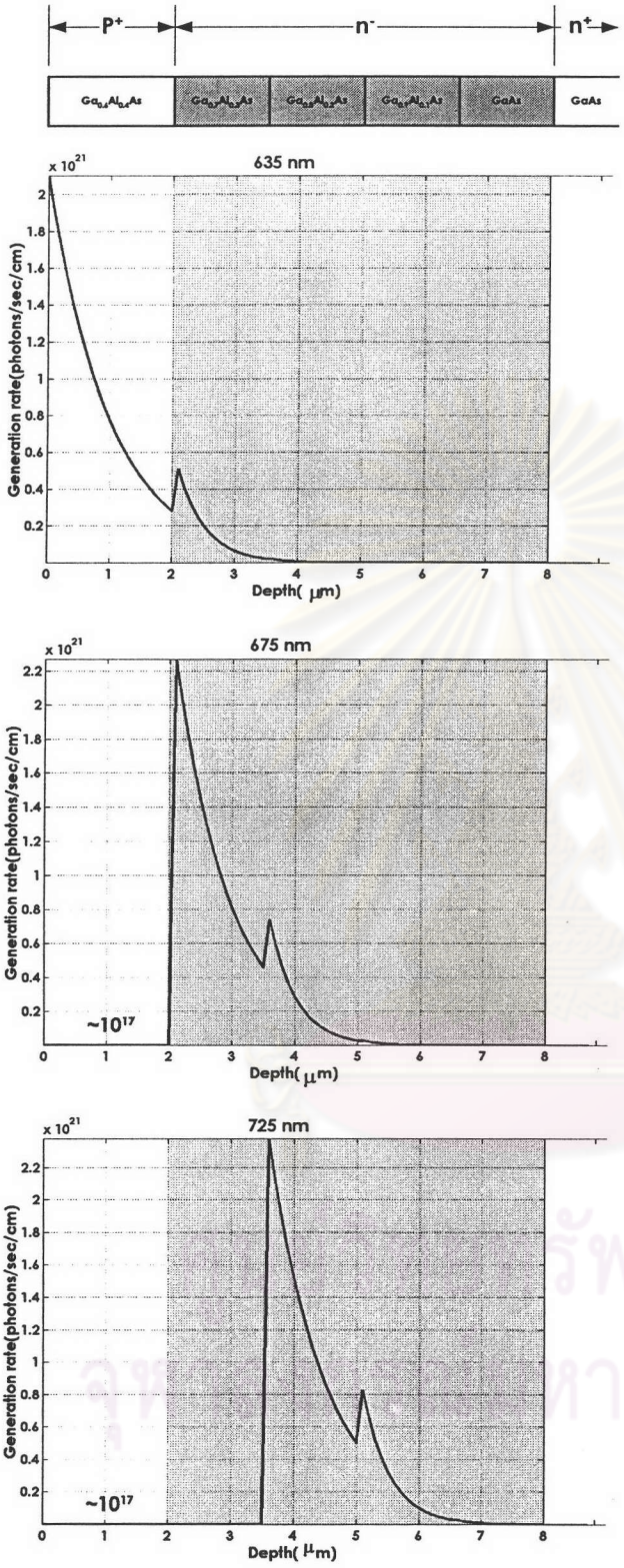

$$J_{dr}(635nm) = -q\int_{2\mu m}^{8\mu m} G(x)dx$$

$$J_{dr}(675nm) = -q\int_{2\mu m}^{8\mu m} G(x)dx$$

$$J_{dr}(725nm) = -q\int_{2\mu m}^{8\mu m} G(x)dx$$

Fig. 3.11 The EHPs generation rate at 635, 675, 725, 785 and 850 nm of structure A2

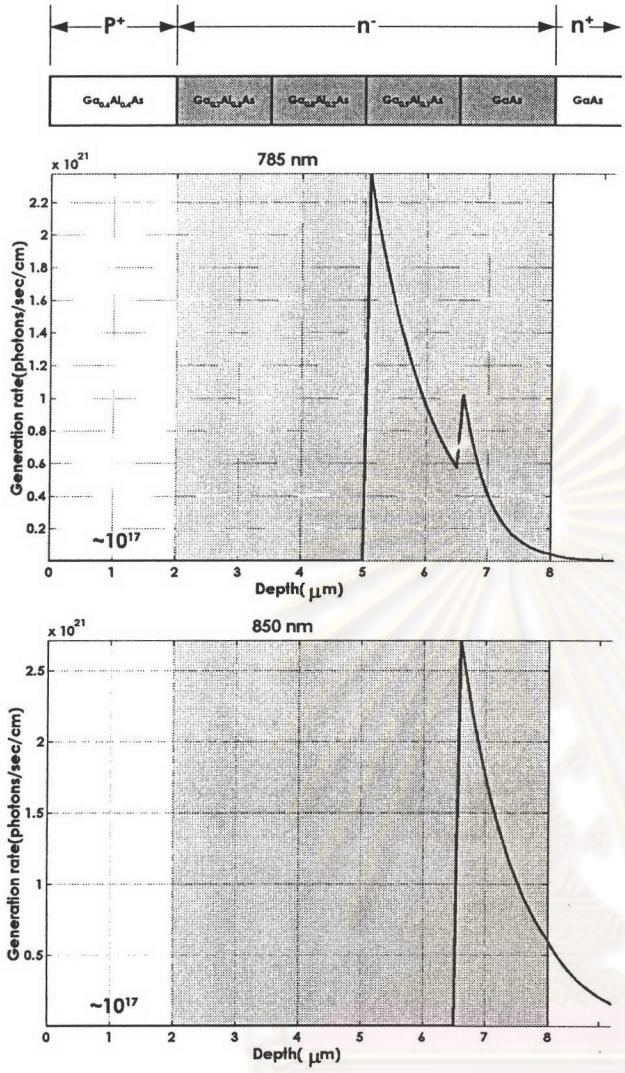

$$J_{dr}(785nm) = -q\int_{2\mu m}^{8\mu m} G(x)dx$$

$$J_{dr}(850nm) = -q\int_{2\mu m}^{8\mu m} G(x)dx$$

Fig. 3.11 (Continued)

Structure A2

The generation rate of the 635 nm optical power is the same as happening in structure A1. In case of 675, 725 and 785 nm, they are nearly the same except the second peaks of these particular generation rates are a little higher than those of the structure A1. This is because each N^- $Ga_{1-x}Al_xAs$ active layer of structure A2 is thinner than that of structure A1. The thinner layer makes the less optical power attenuation; hence the power arriving to the $Ga_{1-x}Al_xAs$ to follow is higher. As for the case of 785 and 850 nm, the generation rates are clearly seen shift to the left and are more absorbed in active region. This is again due to the reasons of the thinner $Ga_{1-x}Al_xAs$ (N^-) layer and also the 1.5 μm GaAs (n^-) layer. The GaAs (n^-) layer itself helps photons of 850 nm to be better absorbed in active region.

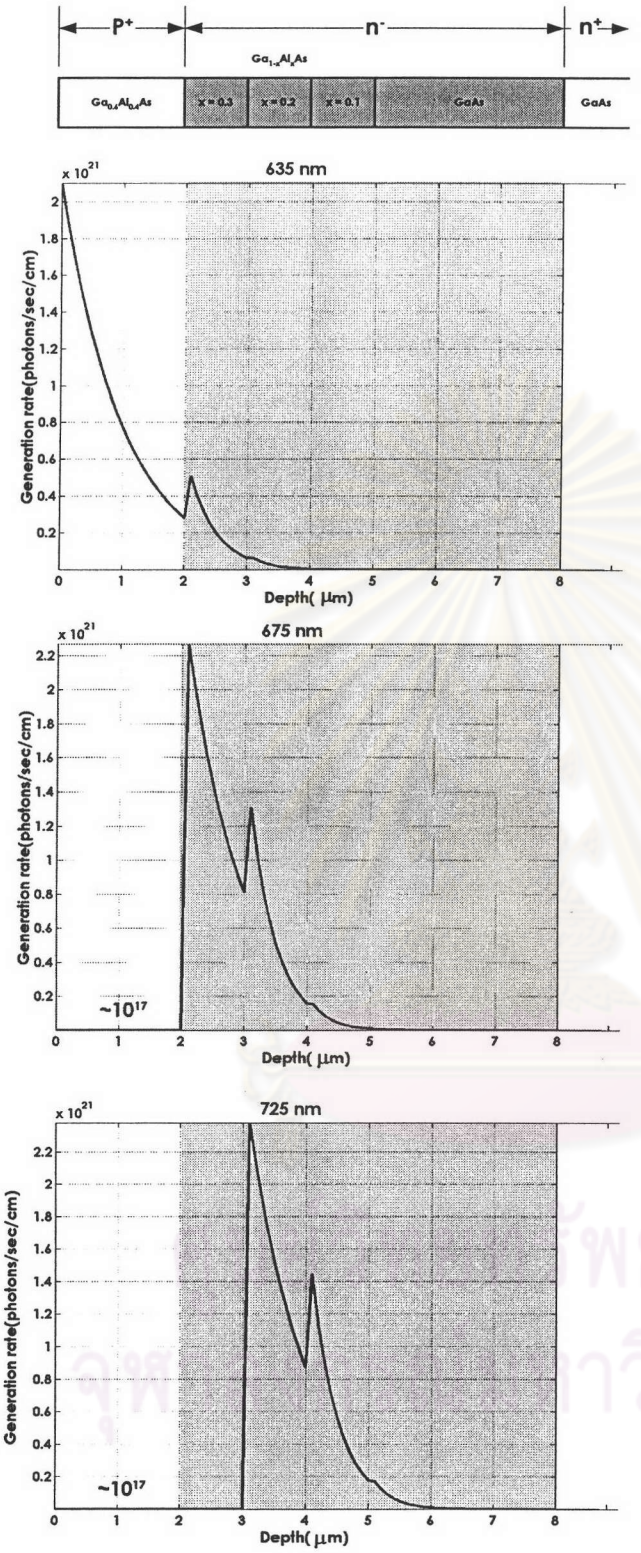

$$J_{dr}(635nm) = -q\int_{2\mu m}^{8\mu m} G(x)dx$$

$$J_{dr}(675nm) = -q\int_{2\mu m}^{8\mu m} G(x)dx$$

$$J_{dr}(725nm) = -q\int_{2\mu m}^{8\mu m} G(x)dx$$

Fig. 3.12 The EHPs generation rate at 635, 675, 725, 785 and 850 nm of structure A3

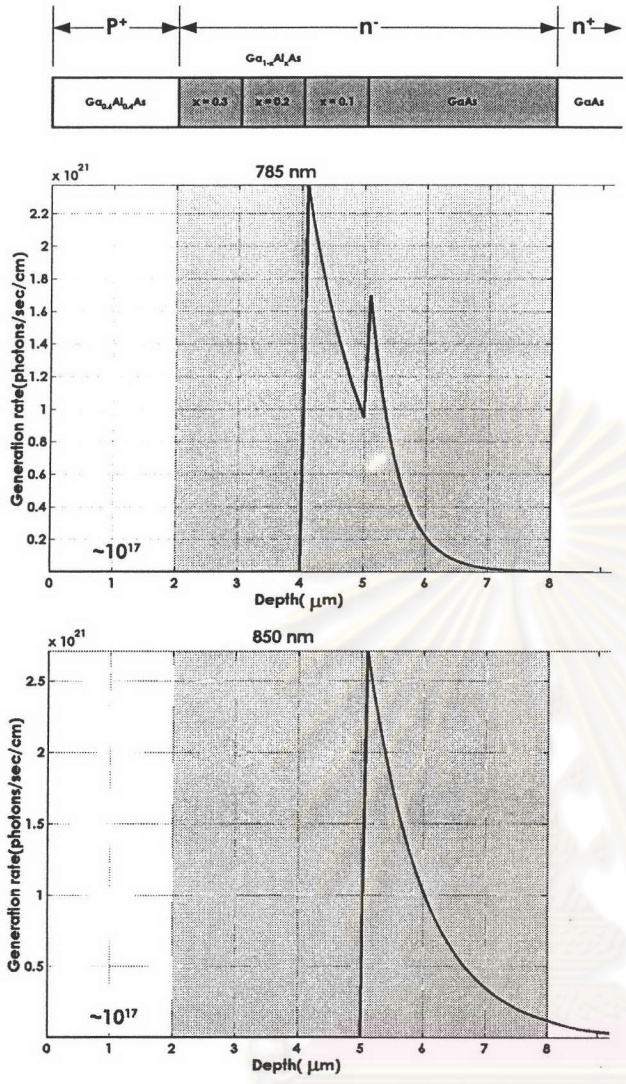

$$J_{dr}(785nm) = -q\int_{2\mu m}^{8\mu m} G(x)dx$$

$$J_{dr}(850nm) = -q\int_{2\mu m}^{8\mu m} G(x)dx$$

Fig. 3.12 (Continued)

Structure A3

In structure A3, the $Ga_{1-x}Al_xAs$ (N^-) layers are adjusted to be thinner whereas the GaAs (n^-) layer is thicker than those of the former structures. The generation rates of 635, 675 and 725 nm are clearly observed with the very small third peak at the interfaces of $Ga_{0.7}Al_{0.3}As/Ga_{0.8}Al_{0.2}As$, $Ga_{0.8}Al_{0.2}As/Ga_{0.9}Al_{0.1}As$ and $Ga_{0.9}Al_{0.1}As/GaAs$ respectively. Actually the discontinuity of generation rate distribution happens whenever the photons travel crossover to the narrower bangap energy layer. According to the 3 μm GaAs (n^-) in active region, all photons of 675, 725 and 785 nm are completely absorbed excluding the generation rate at 850 nm which decreases exponentially with depth across the 3 μm GaAs active layer.

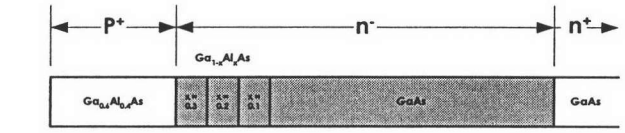

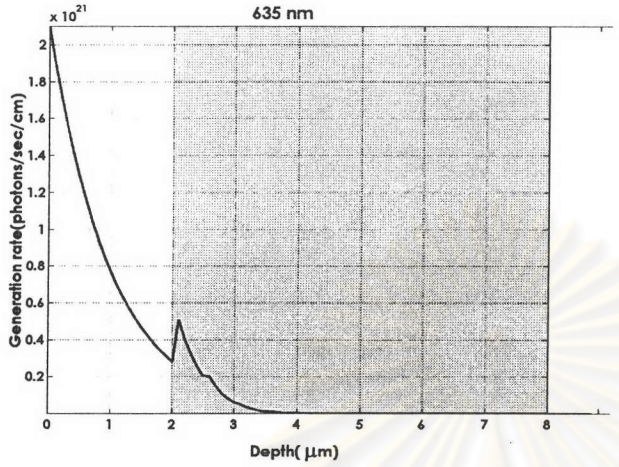

$$J_{dr}(635nm) = -q\int_{2\mu m}^{8\mu m} G(x)dx$$

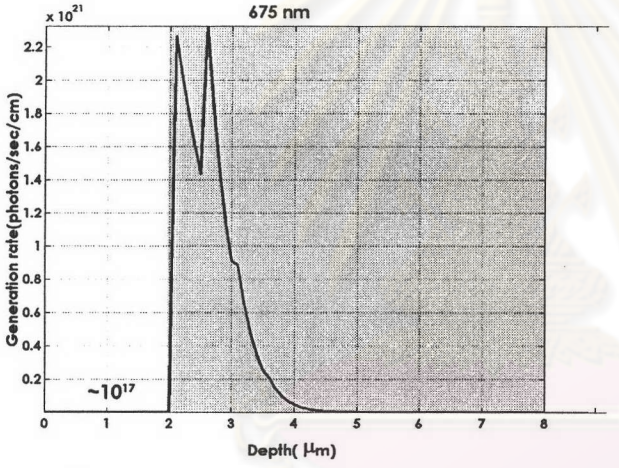

$$J_{dr}(675nm) = -q\int_{2\mu m}^{8\mu m} G(x)dx$$

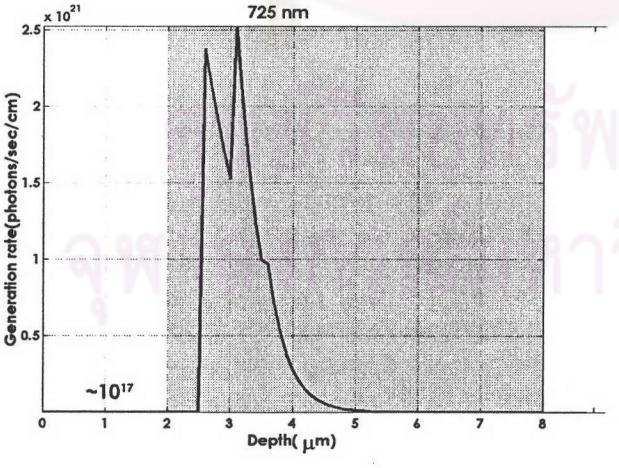

$$J_{dr}(725nm) = -q\int_{2\mu m}^{8\mu m} G(x)dx$$

Fig. 3.13 The EHPs generation rate at 635, 675, 725, 785 and 850 nm of structure A4

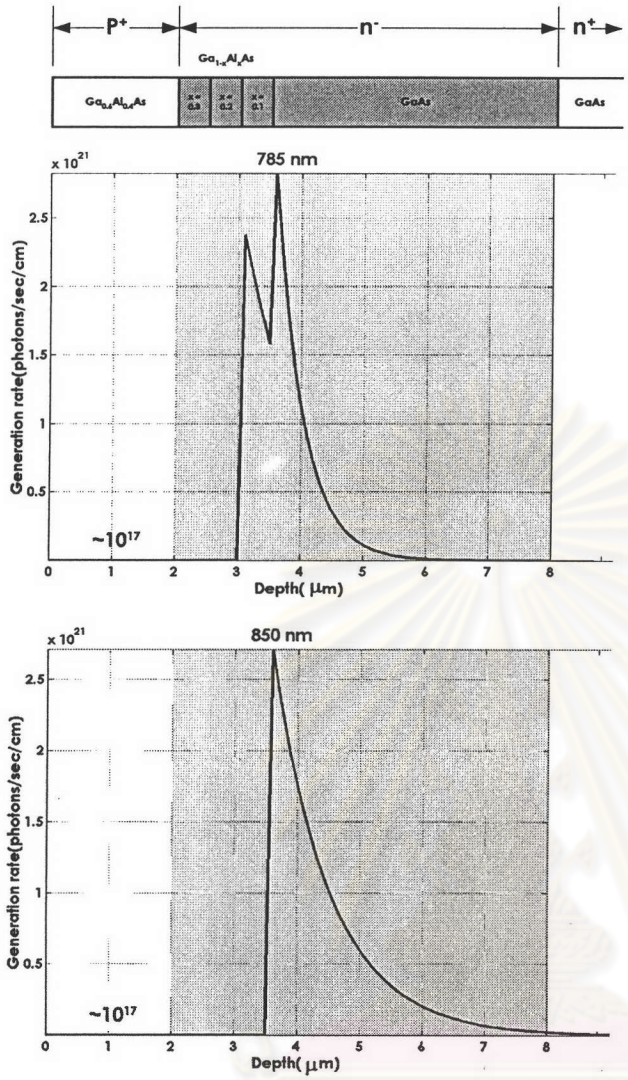

$$J_{dr}(785nm) = -q\int_{2\mu m}^{8\mu m} G(x)dx$$

$$J_{dr}(850nm) = -q\int_{2\mu m}^{8\mu m} G(x)dx$$

Fig. 3.13 (Continued)

Structure A4

This structure is designed with the thinnest $Ga_{1-x}Al_xAs$ (N^-) layers and the thickest GaAs (n^-) layer. The generation rates at 675, 725 and 785 nm are similar to those of structure A3 except that the second peak starts to be higher than the first and more and more for longer wavelength. This is again due to the thinner $Ga_{1-x}Al_xAs$ comparing to the former structure. As in the case of 850 nm, the generation rate starts at the interface of $Ga_{0.9}Al_{0.1}As$/GaAs and have exactly the same generation rate as structure A3.

3.4.2.2 The calculated spectral response

The calculated spectral response of each structure is depicted in Fig. 3.14. In case of structure A1, the spectral response cuts off at approximately 800 nm because the lowest bandgap energy of active region is of $Ga_{0.9}Al_{0.1}As$. Therefore only the photon energy greater than the bangap of $Ga_{0.9}Al_{0.1}As$ is absorbed, which is corresponding to the cutoff wavelength 800 nm. As for structure A2, A3 and A4, their spectral response cutoff at approximately 870 nm which is corresponding to the cutoff wavelength of GaAs (n^-) active layer. Even though structure A2 has the GaAs (n^-) active layer but it is not thick enough to absorb photons (as seen in the generation rate at 850 nm of Fig. 3.11), therefore the cutoff spectral response is not as sharp as the one of structure A3 and A4.

The comparison of calculated spectral response between type A structures is shown in Fig. 3.15. It is clearly seen that the GaAs (n^-) thickness has an influence in the spectral response. The cutoff spectral response becomes sharper as the GaAs (n^-) active layer is adjusted thicker.

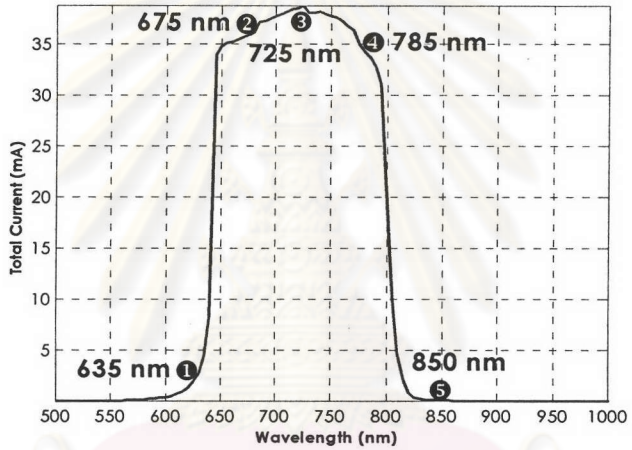

Structure A1

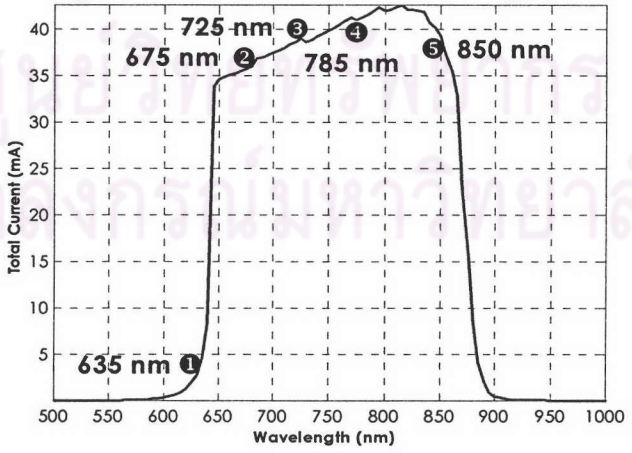

Structure A2

Fig. 3.14 The calculated spectral response of structure A1 to A4

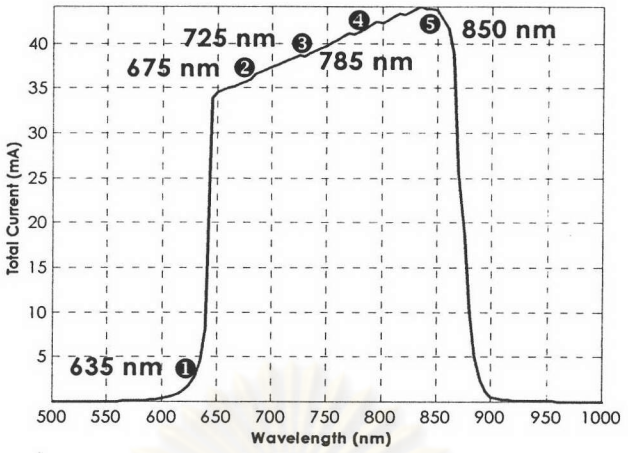

Structure A3

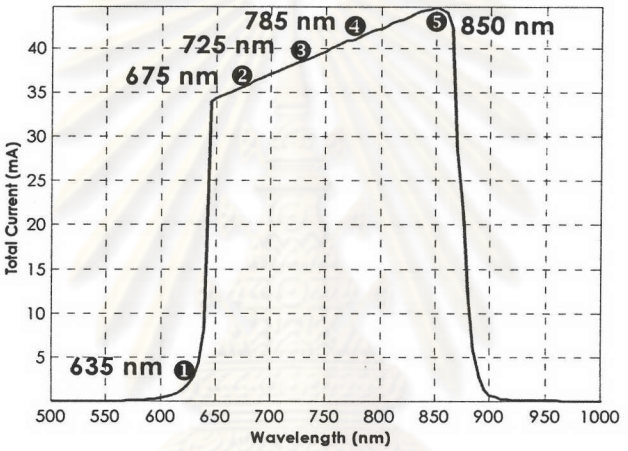

Structure A4

Fig. 3.14 (Continued)

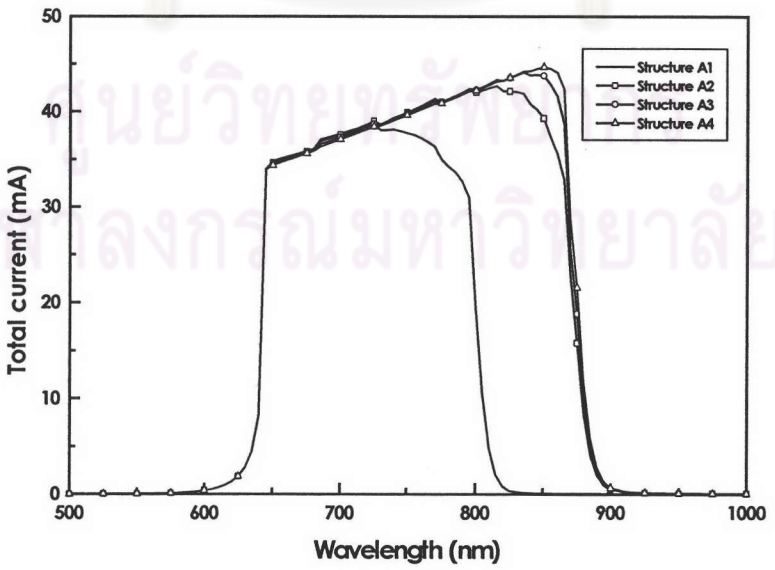

Fig. 3.15 A comparison of calculated spectral response between type A structures

3.4.2.3 The band diagram

The band diagram of type A staircase bangap structure is shown in Fig. 3.16. The advatage of this structure over the constant bandgap structure is that the active layer itself has three conduction band discontinuities which can force electrons to drift downhill toward the n-side. Anyway the small valence band discontinuities themselves are not encouraging the holes to flow smoothly.

3.4.2.4 Application

We will re-discuss the absorption coefficient and the calculated generation rate again, but in the domain of depth. According to the objective of this particular structure is to converge the bandgap energy of active layer from that of window layer to that of GaAs (n^+) substrate. The active layers are therefore in order of $Ga_{0.7}Al_{0.3}As$, $Ga_{0.8}Al_{0.2}As$, $Ga_{0.9}Al_{0.1}As$ and GaAs from the window layer side. Thus, the absorption coefficient of these layers is higher and higher in sequence of the depth. The GaAs which has highest absorption coefficient has the very high generation rate comparing to the one of the other active layers. Hence, the EHPs which are almost generated in this particular layer, are far away from the junction of $Ga_{0.6}Al_{0.4}As$ (P^+) and $Ga_{0.7}Al_{0.3}As$ (N^-) which has very high surface recombination. In addition, electrons can be easily flow toward the n-side of the device due to the GaAs (n^-) active layer is placed nearby the GaAs (n^+) substrate. Nevertheless, holes have to flow far distance toward the p-side.

Under the assumption that $\eta_i = 1$, all absorbed photons can generate the EHPs and all carriers contribute to the current, therefore the spectral response of structure A1to A4 is getting better and better. Nevertheless, we realize that $\eta_i \neq 1$, thus we can use the quasi-electric field to increase the η_i. The quasi-electric fields which are generated from the gradient of the band edge, are working on separating electrons and holes and sweeping those carriers toward the n-side and p-side respectively. For this reason, the photovoltaic effect must be getting better and therefore the η_i increases closely to unity.

The other application of type A staircase bandgap structure is that we can mainly adjust the quasi-electric field especially for electron, which the electron multiplication can be gained. However, the quasi-electric field for hole can rather be adjusted by doping aspect but not as much as the one of electron as seen schematically in Fig. 3.17. The separately adjusted quasi-electric field will greatly benefit for the Separate Absorption and Multiplication (SAM) APD that allows the multiplication to be initiated by one type of carrier. For the sake of this, the excess avalanche noise is reduced to minimum.

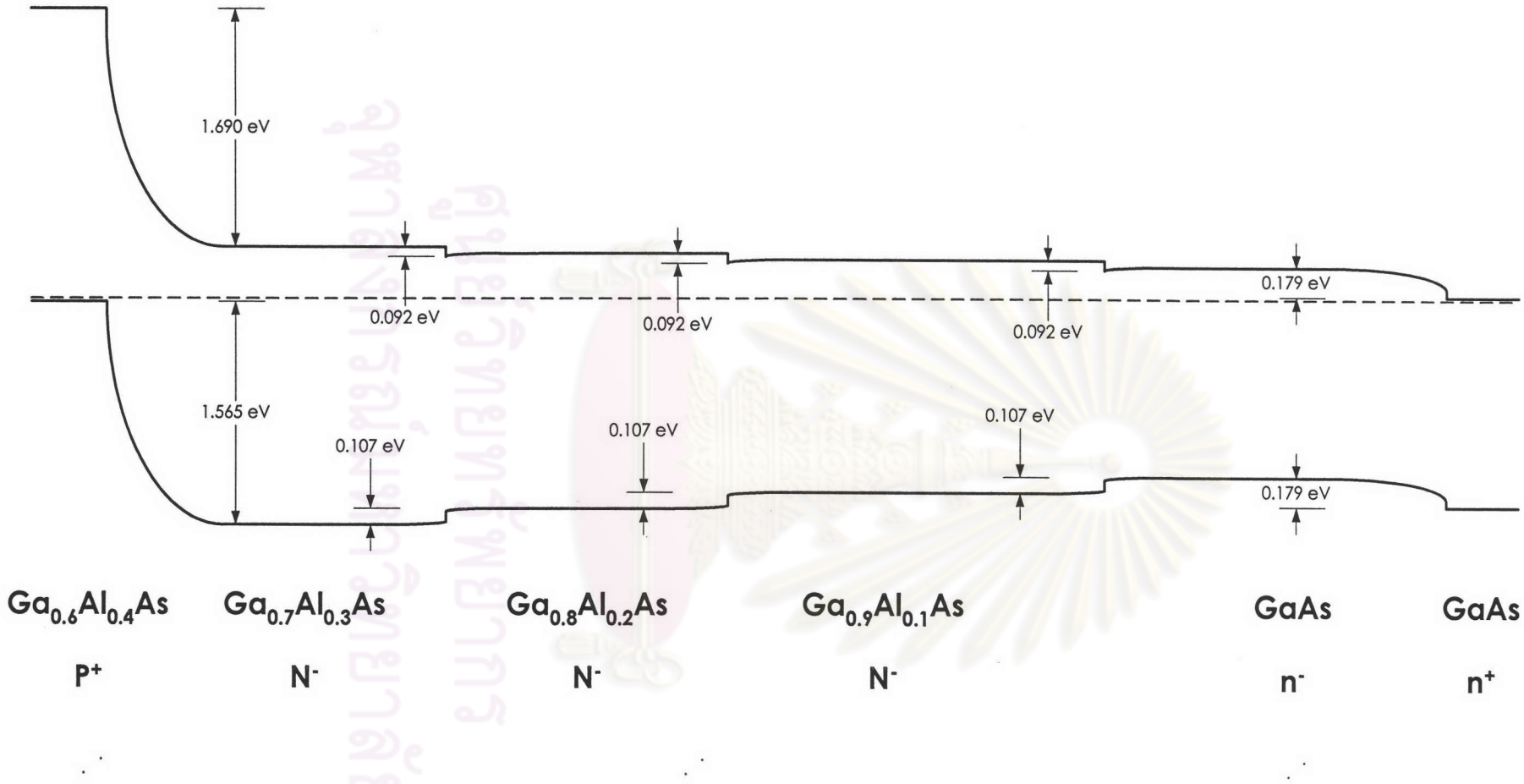

Fig. 3.16 Band diagram of type A staircase bandgap structure

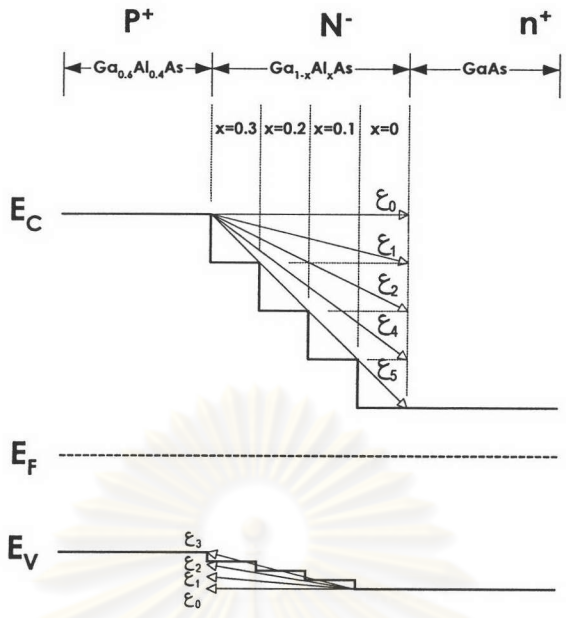

Fig. 3.17 The application of type A staircase bandgap structure

3.4.3 Type B staircase bandgap structure

The staircase bandgap structure type B is also classified into four namely: Structure B1, Structure B2, Structure B3 and Structure B4 as shown in Fig. 3.18. The objective of these structures is opposite to the one of structure A. That is to diverge the bandgap energy of active layer from that of GaAs (n^-) layer underneath the P^+ window layer to that of $Ga_{0.6}Al_{0.4}As$ (N^-) layer near to the GaAs (n^+) substrate. The active layer of each structure is composed of GaAs, $Ga_{0.9}Al_{0.1}As$, $Ga_{0.8}Al_{0.2}As$, $Ga_{0.7}Al_{0.3}As$ and $Ga_{0.6}Al_{0.4}As$ in sequence from the top and with different thickness but all are doped at 10^{15} cm^{-3}. According to structure B1 to B4 in order, the thickness of GaAs (n^-) layer is adjusted to be 1 μm thicker for a time from 0 to 3 μm while the thickness of $Ga_{1-x}Al_xAs$ is adjusted to be 0.25 μm thinner for a time from 1.5 to 0.75 μm. However, the thickness of the window layer and the total active layer are also respectively remained at 2 and 6 μm.

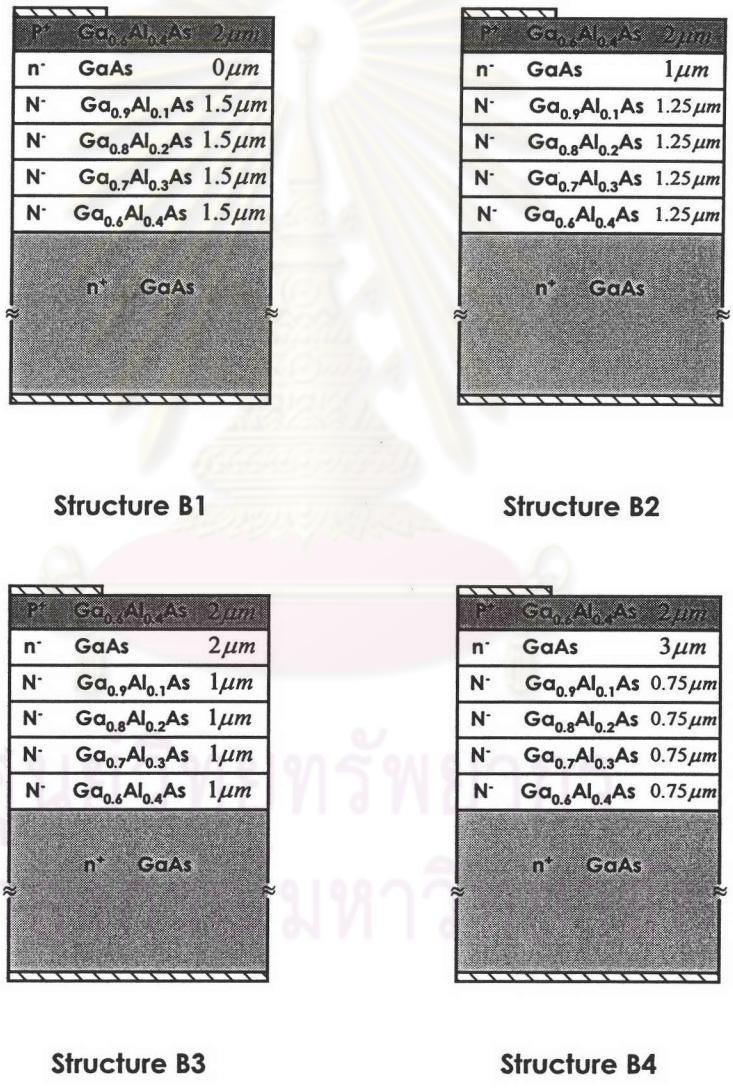

Fig. 3.18 Type B staircase bandgap structures

3.4.3.1 The calculated EHPs generation rate

To have an understanding of the optical absorption mechanism, the generation rates are again calculated at 635, 675, 725, 785 and 850 nm for every structure to compare to the one of constant bandgap. The calculated results are depicted in Fig. 3.19 to 3.22 for structure B1 to B4 respectively. The distribution of these generation rates will be discussed and compared to each other as follows:

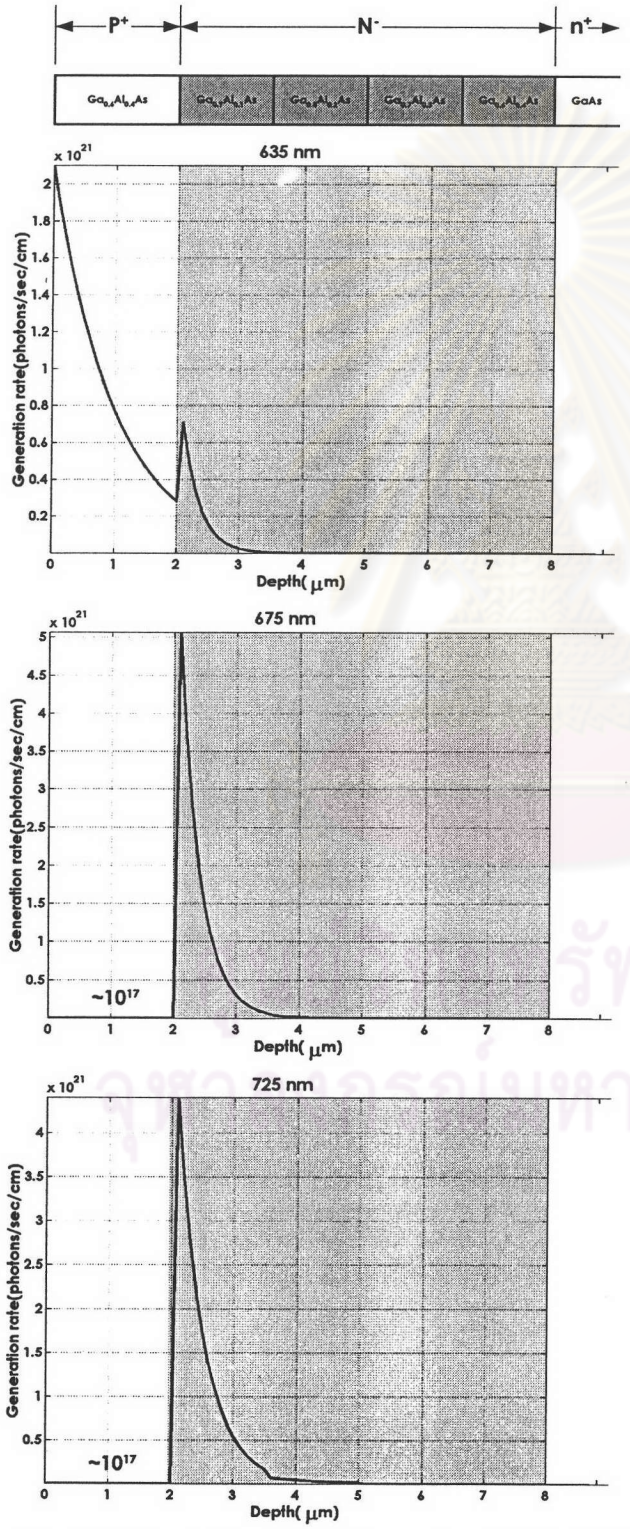

$$J_{dr}(635nm) = -q\int_{2\mu m}^{8\mu m} G(x)dx$$

$$J_{dr}(675nm) = -q\int_{2\mu m}^{8\mu m} G(x)dx$$

$$J_{dr}(725nm) = -q\int_{2\mu m}^{8\mu m} G(x)dx$$

Fig. 3.19 The EHPs generation rate at 635, 675, 725, 785 and 850 nm of structure B1

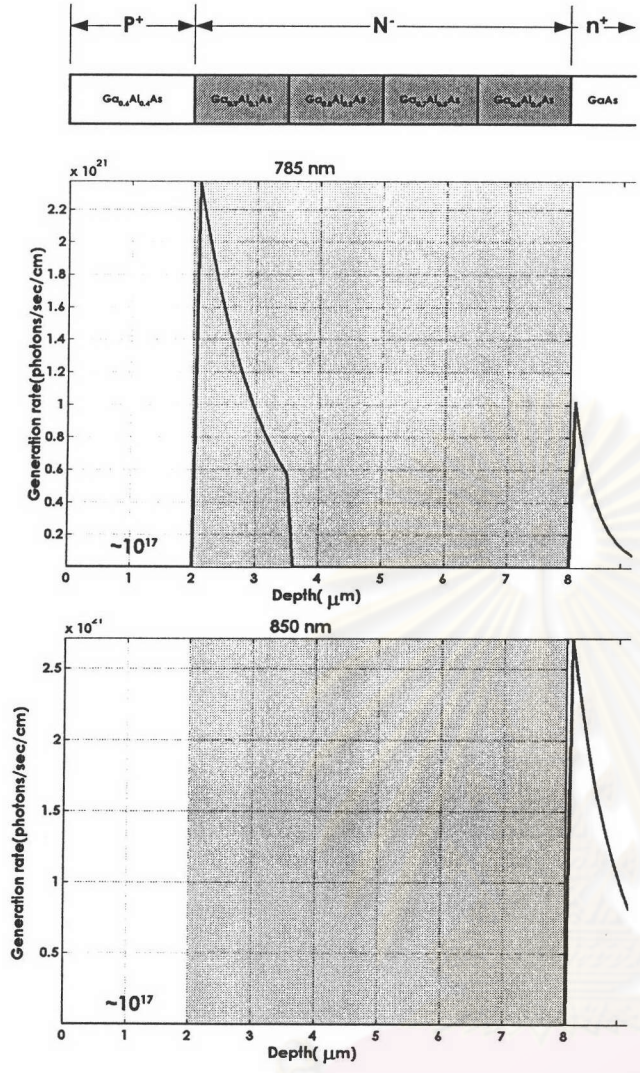

$$J_{dr}(785nm) = -q\int_{2\mu m}^{8\mu m} G(x)dx$$

$$J_{dr}(850nm) = -q\int_{2\mu m}^{8\mu m} G(x)dx$$

Fig. 3.19 (Continued)

Structure B1

In this structure, the 635 nm optical power is very much absorbed inside the surface layer and decreases exponentially with depth as the one of the constant bandgap structure. The different is that the height of second peak of this particular generation rate decreases a little bit since the first active layer of structure B1 is $Ga_{0.9}Al_{0.1}As$ in place of GaAs. As for the other energies, they are also absorbed less than those of the reference structure because of the lower absorption coefficient of $Ga_{0.9}Al_{0.1}As$. Note that these generation rates do not show the second peak as in the case of 635 nm due to the absorption coefficient of staircase bandgap active layer changes lower to lower from that of $Ga_{0.9}Al_{0.1}As$ to that of $Ga_{0.6}Al_{0.4}As$. For this reason, such generation rates fall down whenever passing to the next layer as clearly seen in case of 725 and 785 nm. Especially in case of 785 nm, the photons cannot entirely be absorbed in $Ga_{0.9}Al_{0.1}As$ active layer; therefore the rest is absorbed in the substrate. Since this structure does not have the GaAs (n^-) layer, the photon power of 850 nm prefers not to be absorbed in active region but is absorbed in GaAs (n^+) substrate.

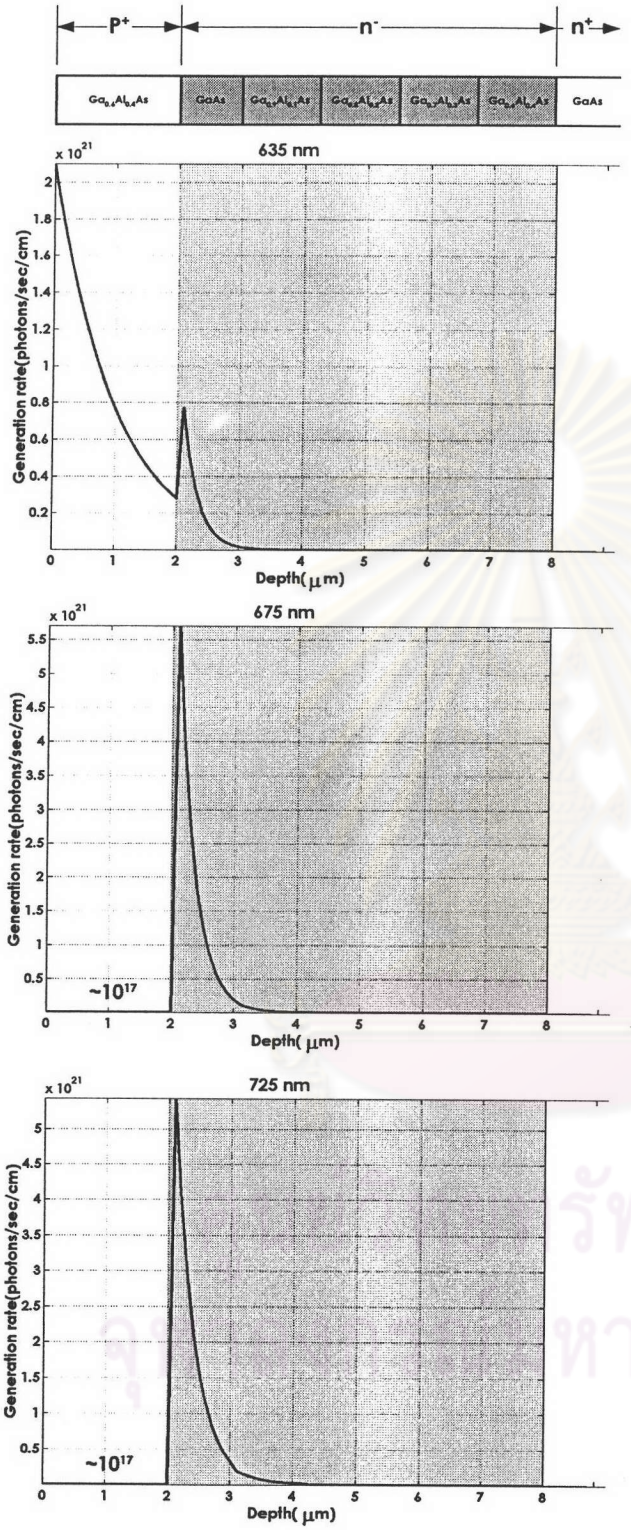

$$J_{dr}(635nm) = -q\int_{2\mu m}^{8\mu m} G(x)dx$$

$$J_{dr}(675nm) = -q\int_{2\mu m}^{8\mu m} G(x)dx$$

$$J_{dr}(725nm) = -q\int_{2\mu m}^{8\mu m} G(x)dx$$

Fig. 3.20 The EHPs generation rate at 635, 675, 725, 785 and 850 nm of structure B2

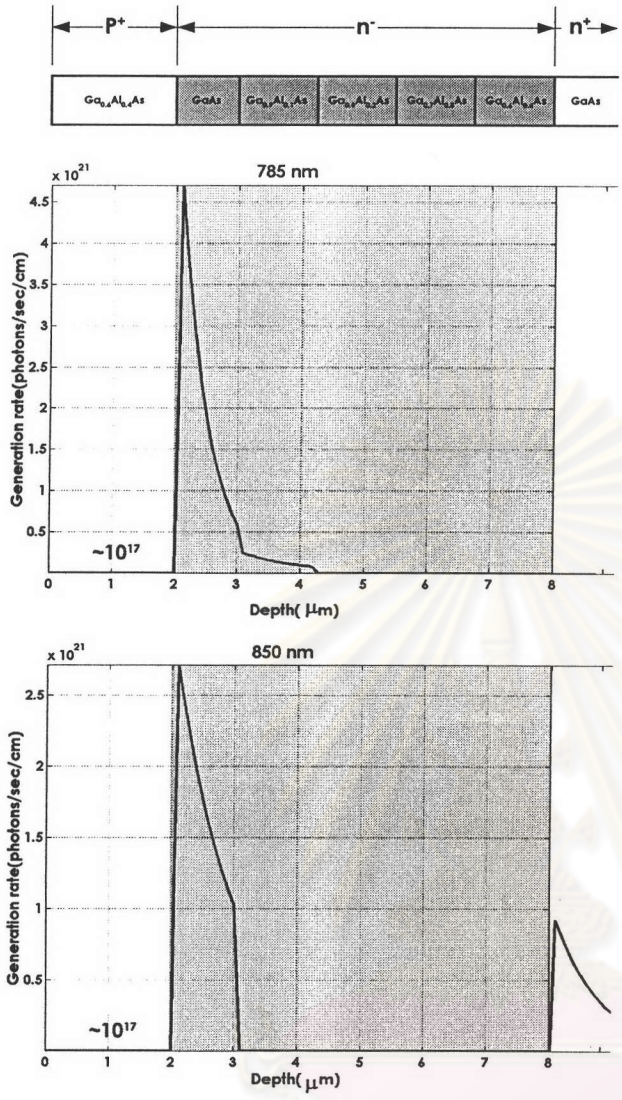

$$J_{dr}(785nm) = -q\int_{2\mu m}^{8\mu m} G(x)dx$$

$$J_{dr}(850nm) = -q\int_{2\mu m}^{8\mu m} G(x)dx$$

Fig. 3.20 (Continued)

Structure B2

In this structure, the generation rates of 635, 675 and 725 nm are similar to those of structure B1 but higher because structure B2 has the higher absorption coefficient of GaAs (n^-) active layer. For the case of 785 nm optical power, the generation rate distributes exactly to the one of 725 nm of structure B1. This is again because the absorption coefficient of the layer to follow ($Ga_{0.9}Al_{0.1}As$) changes to lower. In case of 850 nm, some photons can pass through the active layer into the substrate and consequently not contribute to the drift current. This is because the GaAs active layer is not thick enough.

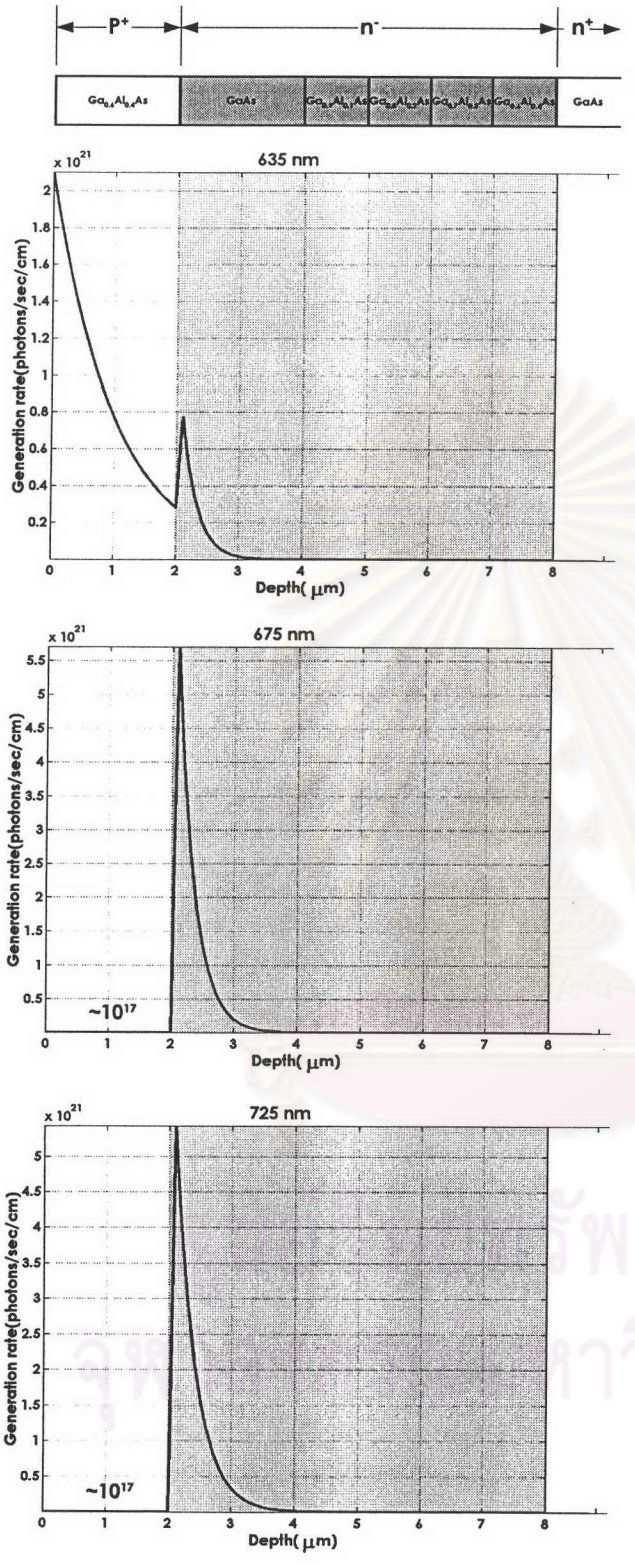

$$J_{dr}(635nm) = -q\int_{2\mu m}^{8\mu m} G(x)dx$$

$$J_{dr}(675nm) = -q\int_{2\mu m}^{8\mu m} G(x)dx$$

$$J_{dr}(725nm) = -q\int_{2\mu m}^{8\mu m} G(x)dx$$

Fig. 3.21 The EHPs generation rate at 635, 675, 725, 785 and 850 nm of structure B3

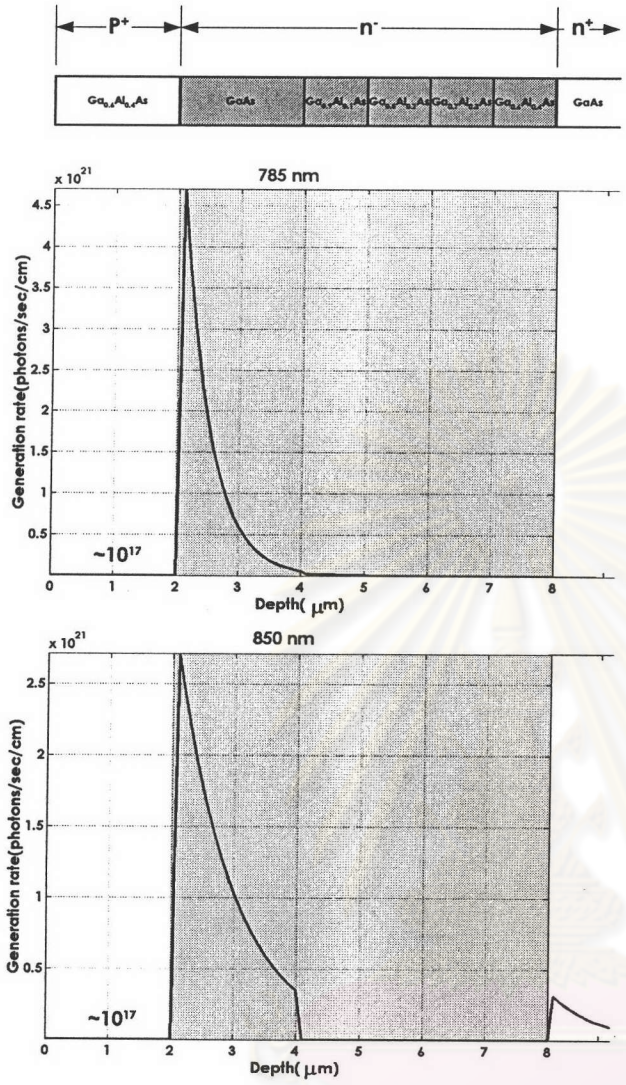

$$J_{dr}(785nm) = -q\int_{2\mu m}^{8\mu m} G(x)dx$$

$$J_{dr}(850nm) = -q\int_{2\mu m}^{8\mu m} G(x)dx$$

Fig. 3.21 (Continued)

Structure B3

In structure B3, the GaAs (n^-) layer is adjusted thicker whereas the $Ga_{1-x}Al_xAs$ (N^-) layers are thinner than those of the former structures. Therefore, all generation rates are higher and distribute quite similar to those of structure B2. It is observed that the 850 nm optical power that is absorbed more in active layer because of 2 μm GaAs (n^-) active layer.

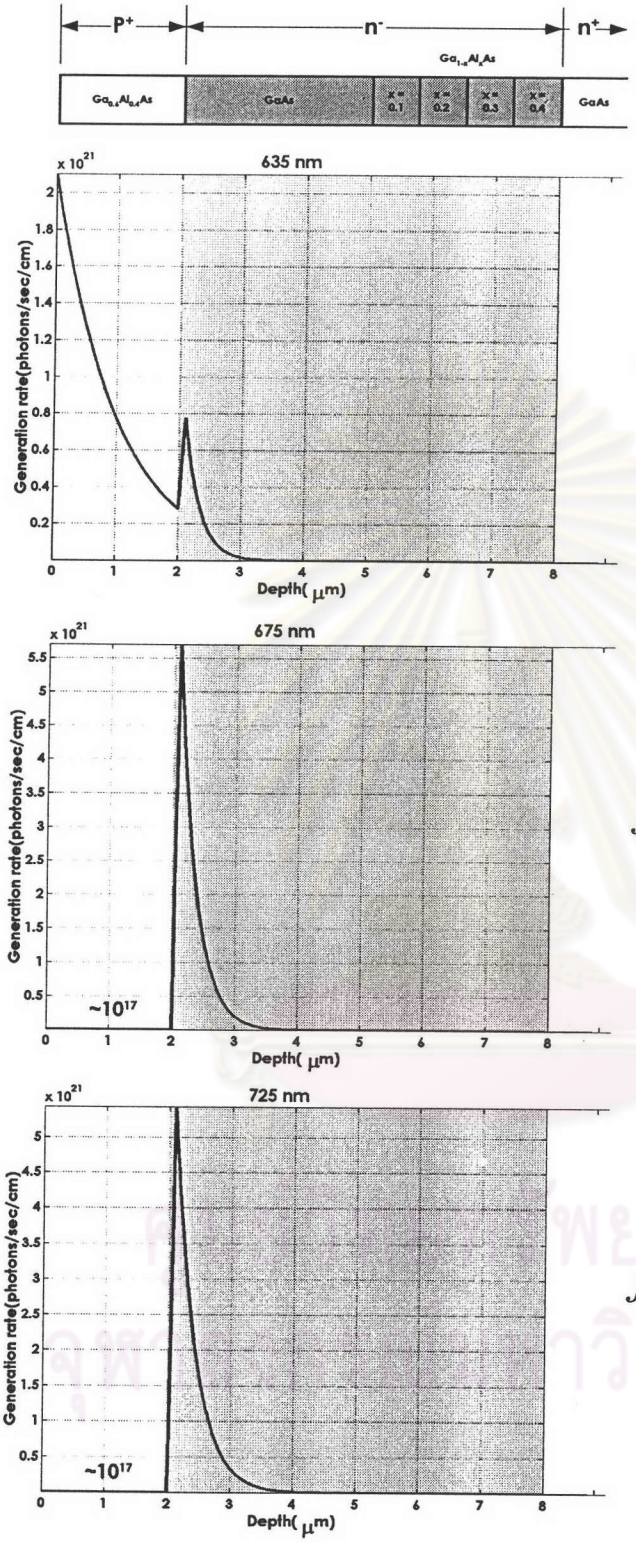

$$J_{dr}(635nm) = -q\int_{2\mu m}^{8\mu m} G(x)dx$$

$$J_{dr}(675nm) = -q\int_{2\mu m}^{8\mu m} G(x)dx$$

$$J_{dr}(725nm) = -q\int_{2\mu m}^{8\mu m} G(x)dx$$

Fig. 3.22 The EHPs generation rate at 635, 675, 725, 785 and 850 nm of structure B4

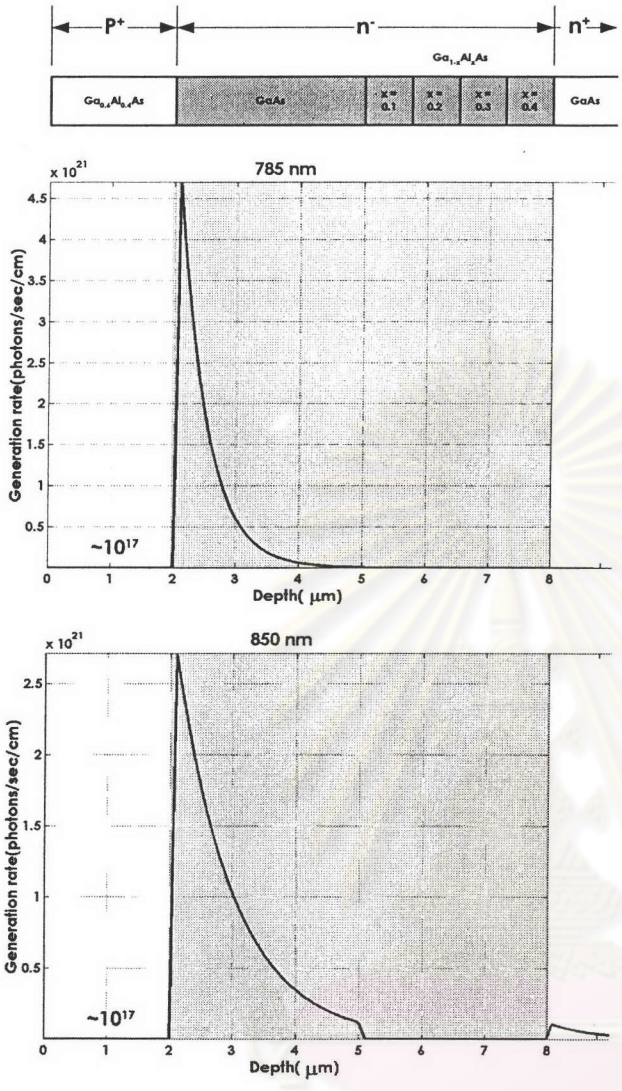

$$J_{dr}(785nm) = -q\int_{2\mu m}^{8\mu m} G(x)dx$$

$$J_{dr}(850nm) = -q\int_{2\mu m}^{8\mu m} G(x)dx$$

Fig. 3.21 (Continued)

Structure B4

This structure is designed with the thickest GaAs (n^-) layer and the thinnest $Ga_{1-x}Al_xAs$ (n^-) layers. Again and again, all generation rates are similar to those in structure B3 and also the 850 nm is absorb more and more in active layer because of the thicker GaAs (n^-) layer comparing to the former structure. Note that the photon energy would prefer to absorb only in the GaAs (n^-) active layer than the others. This is because the higher absorption coefficient it is.

3.4.3.2 The calculated spectral response

The calculated spectral response of each structure is depicted in Fig. 3.22. In case of structure B1, the spectral response cuts off at approximately 800 nm because the lowest bandgap energy of active layer is of $Ga_{0.9}Al_{0.1}As$. Therefore only the photon energy greater than the bangap energy of $Ga_{0.9}Al_{0.1}As$ is absorbed, which is corresponding to the cutoff wavelength at 800 nm. As for structure B2, B3 and B4, their spectral response cutoff at approximately 870 nm which is corresponding to the cutoff wavelength of GaAs (n^-) active layer. Note that the lowest bandgap energy active layer dominates the optical power absorption which is the $Ga_{0.9}Al_{0.1}As$ (N^-) layers in case of structure B1 while the GaAs (n^-) layer does for structure B2, B3 and B4.

The comparison of calculated spectral response between type B structures is shown in Fig. 3.23. This is again that the GaAs (n^-) thickness has an influence in the spectral response. The cutoff spectral response becomes sharper as the GaAs (n^-) active layer is adjusted thicker.

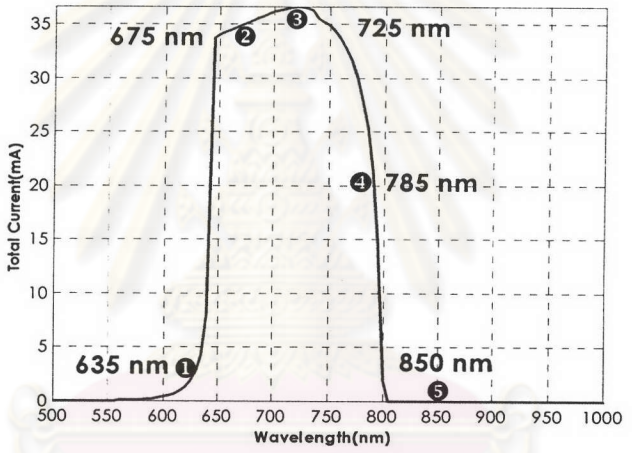

Structure B1

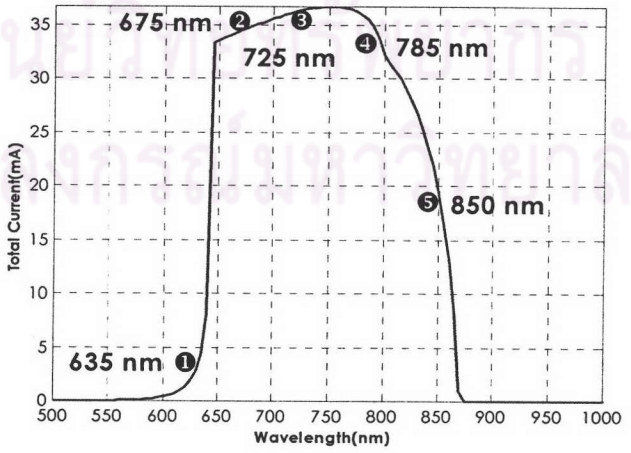

Structure B2

Fig. 3.22 The calculated spectral response of structure B1 to B4

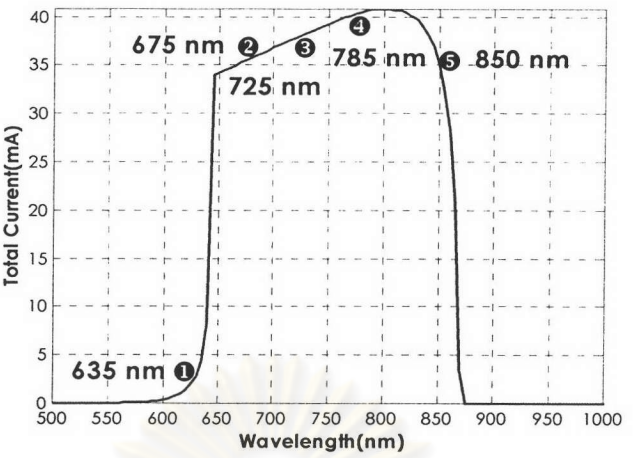

Structure B3

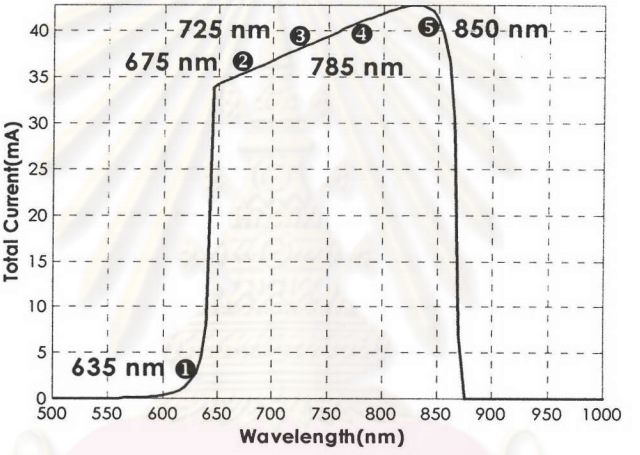

Structure B4

Fig. 3.22 (Continued)

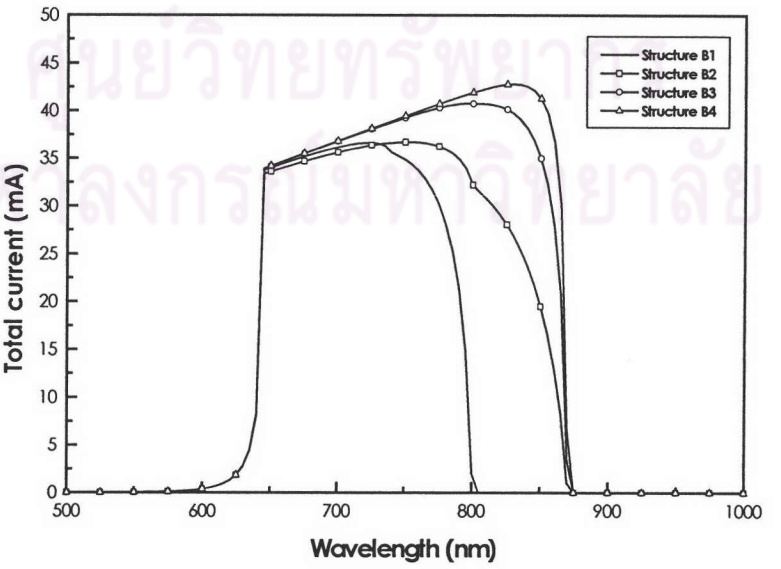

Fig. 3.23 A comparison of calculated spectral response between type B structures

3.4.3.3 The band diagram

The band diagram of staircase bangap structure type B is shown in Fig. 3.24. The advatage of this structure over the constant bandgap structure is that the active layer itself has three valence band discontinuities, which the quasi-electric field for hole can be generated and therefore holes can be forced to sweep downhill toward the n-side. Anyway the barrier on the valence band due to the GaAs (n^-) active layer and the small barriers in conduction band can be minimized by the doping aspect.

3.4.3.4 Application

According to The objective of these structures is to diverge the bandgap energy of active layer from that of GaAs (n^-) layer underneath the P^+ window layer to that of $Ga_{0.6}Al_{0.4}As$ (N^-) layer near to the n^+ substrate. The active layers are therefore in order of GaAs, $Ga_{0.9}Al_{0.1}As$, $Ga_{0.8}Al_{0.2}As$, $Ga_{0.7}Al_{0.3}As$ and $Ga_{0.6}Al_{0.4}As$ from the window layer side. Thus, the absorption coefficient of these layers is lower and lower in sequence of the depth. The GaAs which has highest absorption coefficient, has the very high generation rate compares to the one of the other active layers. Hence, the big problem of these structures is that the EHPs which are almost generated in this particular layer, are very closed to the junction of $Ga_{0.6}Al_{0.4}As$ (p^+) and GaAs (n^-) which has very high surface recombination as happening in the constant bandgap structure. Nevertheless, electrons have to flow far distance toward the n-side. However, the only advantage of these structures is that holes can be easily flow toward the p-side of the device due to the GaAs (n^-) active layer is placed nearby the $Ga_{0.6}Al_{0.4}As$ (p^+) window layer.

Under the assumption that $\eta_i = 1$, all absorbed photons can generate the EHPs and all carriers contribute to the current, therefore the spectral response of structure B1to B4 is getting better and better. Nevertheless, we realize that $\eta_i \neq 1$, thus we can use the quasi-electric field to increase the η_i. The quasi-electric fields which are generated from the gradient of the band edge, are working on separating electrons and holes and sweeping those carriers toward the n-side and p-side respectively. For this reason, the photovoltaic effect must be getting better and therefore the η_i is increased closely to unity.

The other application of type B staircase bandgap structure is that we can mainly adjust the quasi-electric field especially for holes, which the hole multiplication can be gained. However, the quasi-electric field for electron can rather be adjusted by doping aspect but not as much as the one of hole as seen schematically in Fig. 3.25. The separately adjusted quasi-electric field will greatly benefit for the SAM APD. For the sake of this, the excess avalanche noise is reduced to minimum.

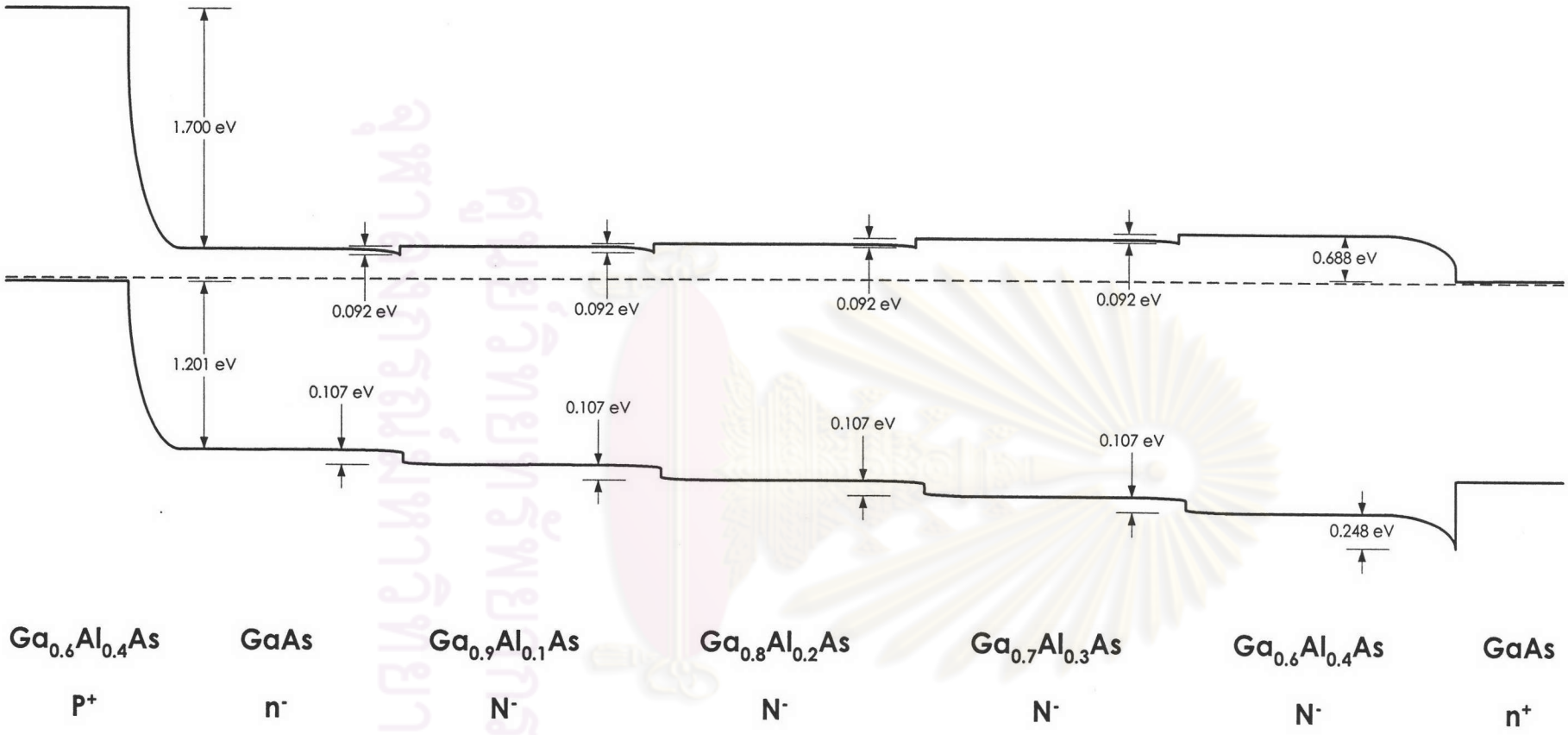

Fig. 3.24 Band diagram of type B staircase bandgap

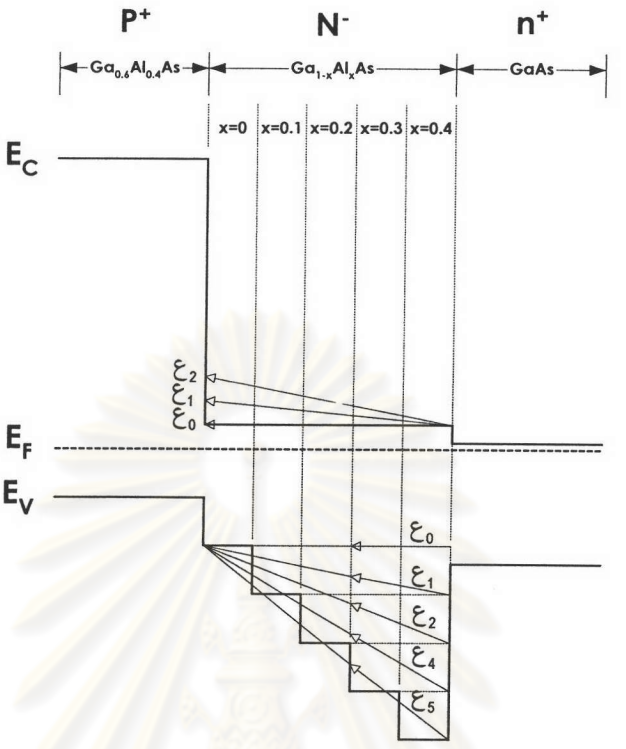

Fig. 3.25 The application of type B staircase bandgap sturcture